IN SITU ASSESSMENT OF ENGINE OIL QUALITY THROUGH REAL-TIME SENSING

By

Cameron Jacob Schepner

Thesis

Submitted to the Faculty of the

Graduate School of Vanderbilt University

in partial fulfillment of the requirements

for the degree of

MASTER OF SCIENCE

in

MECHANICAL ENGINEERING

May 12, 2023

Nashville, Tennessee

Approved:

Amrutur Anilkumar, Ph.D.

Robert Pitz, Ph.D.

E. Duco Jansen, Ph.D.

ACKNOWLEDGMENTS

I would like to thank my parents, Rob and Karen, for enabling me to succeed. They put me in a position that allowed me to get to where I am today, and for that I will be forever grateful.

I would also like to thank my advisor, Dr. Amrutur Anilkumar, for his incredible efforts and long hours spent mentoring me and molding me into a well-rounded engineer. Without his support and the opportunities he gave me, I would consider my engineering education incomplete. Additionally, I would like to thank Dr. Robert Pitz and Dr. Duco Jansen for their willingness to participate as members of my thesis committee.

This research was funded in part by the Mark Dalton Vanderbilt Aerospace Design Laboratory fund.

TABLE OF CONTENTS

Page

LIST OF FIGURES . . . . . **v**

1 Executive Summary **1**

2 Investigation of Lubricant Flow Characteristics in the Engine **2**

2.1 Background 2
2.2 Experiment Design 3
2.2.1 Testbed Diesel Engine Facility 3
2.2.2 Flow Cell Design and Evaluation 3
2.2.3 Imaging System and Image Processing Technique 5
2.2.4 Flow Cell Implementation at the Engine 6
2.3 Flow Visualization Results 8
2.4 Interpretation of Flow Characteristics 13

3 Evaluation of Oil Quality Sensor (OQS) in the Benchtop Flow Facility **14**

3.1 Background 14
3.2 Benchtop Facility and Experimental Procedure 15
3.3 Oil Quality Sensor Measurement Characteristics 20
3.3.1 Run-to-Run Measurement Repeatability 20
3.3.2 Loss Factor Response to Temperature Change 20
3.3.3 Loss Factor Response to OQS Radial Orientation 21
3.3.4 Hysteresis in Loss Factor Response 22

4 Oil Quality Sensor Implementation on the Diesel Engine **24**

4.1 Engine Brake Loading and Test Procedure 24
4.2 Oil Quality Sensing Results for Used and Clean Oils 26
4.3 Modeling Sensor Response to Temperature in Used and Clean Oils 27
4.4 Investigating Aeration as the Root Cause for Measurement Discrepancy 29

5 Conclusion **33**

References **34**

LIST OF FIGURES

Figure		Page
2.1	Volkswagen 4-cylinder, 1.9L TDI testbed engine facility with dynamometer.	3
2.2	Flow schematic of the stock Volkswagen 1.9L TDI oil filter housing, where orange arrows represent pre-filter flow and green arrows represent post-filter flow.	4
2.3	Oil filter housing assembly with the flow diverter integrated in the pre-filter oil flow line.	4
2.4	CAD rendering of the flow visualization cell.	5
2.5	Oil filter housing and flow visualization test cells incorporated onto the benchtop test facility. The facility is capable of emulating engine operating conditions in a controllable manner. Oil flow temperature is monitored at the entrance and exit of the filter.	5
2.6	Top-down schematic of the backlit imaging setup.	6
2.7	Thresholding sequence of strobe-generated bubble silhouettes in moving oil. (L-R) Raw image, grayscale image, thresholded binary image.	6
2.8	External flow visualization facility integrated into the engine testbed.	7
2.9	Temperature data collected during a typical engine run. The engine brake powers and speeds during operation are denoted.	8
2.10	Typical flow image sequence at 1000 fps, with the engine operating at 2800 rpm and an oil temperature of 224°F. Bubbles used to model flow velocity (Figure 2.11) are highlighted with red circles.	9
2.11	Laminar velocity profile model of the oil flow in the test cell. Points indicate data from image sequence shown in Figure 2.10.	9
2.12	Additional image sequences tracking bubble pairs for flow speed analysis in Figure 2.13.	10
2.13	Average flow profile using data obtained from image sequences in Figures 2.10 and 2.12.	10
2.14	Bubble number density histogram showing a log-normal distribution for typical engine operating conditions of 2800 rpm, 224°F.	11
2.15	Sample of images used to obtain bubble number distribution in flowing oil at an engine speed of 2800 rpm and 224°F.	11
2.16	Sample images taken at an engine speed of 2800 rpm at three different temperatures.	12
2.17	(a) Variation of volumetric aeration percentage with engine speed at constant temperature (220 $\pm$ 5°F). (b) Variation of volumetric aeration percentage with oil temperature at constant engine speed (2800 rpm).	12
2.18	Engine oil sump environment during engine operation.	13
3.1	TanDelta Oil Quality Sensor (OQS) and schematic of sensing tip.	15
3.2	Benchtop facility with major components; red arrows show flow direction. Oil quality sensors can be mounted in both inline test cells as well as the filter housing. The flow meter is just upstream of the oil tank and obscured in the picture.	17
3.3	Oil quality sensors integrated into the modified oil filter housing. (a) Filter housing OQS orientations. (b) Inside view of sensing elements intercepting the oil flow. (c) Oil filter housing with sensors integrated into benchtop test facility (wrapped with thermal insulation).	18
3.4	Window of operation for the benchtop facility, dictated by operational temperature regime of the engine, pump power limit, and minimum flow speed required for thermal uniformity.	19
3.5	Loss factor response to a ramp-up in temperature, with equilibration timescales denoted. Figure from research conducted by Adam Smith [35].	20
3.6	(a) OQS as installed on the oil filter housing tilted at 15°. (b) Schematic of the inline OQS, which can be rotated about the hose axis. Figure from research conducted by Adam Smith [35].	21
3.7	Inline OQS loss factor measurements at various orientation angles. The blue dot represents data collected at the filter location (15° from the vertical). Figure from research conducted by Adam Smith [35].	22
3.8	Results of temperature-based hysteresis study using oil sample B; measurements taken at the vertical filter location in the benchtop.	23

4.1 Vertical OQS as installed at the oil filter housing on the engine. Oil temperature was monitored by the built-in thermistor on the OQS (Figure 3.1). 25
4.2 Sample measurements from a typical engine test run, showing OQS loss factor, OQS oil temperature, and the engine coolant temperature. 25
4.3 Comparison of loss factor measurements collected during engine and benchtop tests for oil sample B. Runs 1 and 2 represent horizontal and vertical OQS configurations of the same sensor. 26
4.4 Comparison of loss factor measurements from clean oil (sample A) tests on the engine and benchtop. 27
4.5 Steady state OQS response to temperature in benchtop experiments, fit with exponential function (equation 4.1). The fit constants A, B, and C were approximately 2.2, 3.9, and 4.5, respectively. 28
4.6 Exponential fits for single sensor data from engine and benchtop experiments for both the clean and used oil samples (samples A and B). 28
4.7 Image of aerated oil flow adjacent to the oil filter in the running engine at 220°F, showing prominent bubble sizes compared to the oil quality sensor's capacitor gap size. 29
4.8 Comparison between pre-filter and post-filter OQS loss factor measurements in a single engine run. 30
4.9 Projection for the volumetric aeration percentage from difference in loss factor measurement. 31
4.10 Oil sample A (clean oil) benchtop data vs. engine data, with the dashed line qualitatively depicting the results of a study with a constant engine speed of 2800 rpm rather than varying engine speed. 32

CHAPTER 1

Executive Summary

This is a two-part study conducted to assess the flow-related factors associated with real-time implementation of permittivity-based engine lubricant oil quality sensors. In the first part of this study, the flow characteristics of clean oil at the chosen sensor location in the engine were visualized prior to the subsequent sensor implementation. Sensor implementation on the engine followed detailed characterization on a benchtop facility emulating engine operating conditions of temperature and flow rate.

Oil quality measurements on the engine showed a systematic difference from similar measurements on the benchtop facility. The presence of aeration through microbubbles in the engine oil flow, as compared with the benchtop oil flow, has been hypothesized to be the reason for the bias in the electrical permittivity measurements, as these bubbles are a consistent part of the sensor's sampling volume.

A simple model for the sensor's permittivity measurement variation with temperature has been used to correlate the difference in measurements between the engine and benchtop facilities with the same working oil. Using this modeling approach, predictions have been made for aeration percentages of used oils based on the combined visualization and measurement results from the clean oils.

The current studies have proved that successful implementation of oil quality sensors in engine oil flows will require systematic characterization of sensor performance under controlled aeration conditions in benchtop facilities with oil samples representing different levels of degradation.

CHAPTER 2

Investigation of Lubricant Flow Characteristics in the Engine

2.1 Background

Engine lubricant quality is critical to the operating health of an engine. Several methods have been developed to measure individual properties of lubricating oil to determine its loss of quality during engine operation [1] including standard chemical tests (total acid number (TAN) and total base number (TBN)), contaminant tests (soot and moisture) [2] [3] [4], viscosity evaluation [5] [6], wear particle sensing, and electrical permittivity sensing [7] [8]. Permittivity-based oil quality sensors measure the complex electrical permittivity of an oil by interrogating a flow region continuously with a high-frequency alternating current. The permittivity of an oil predominantly changes with use due to high temperature oxidative degeneration and the consequent production of polar molecules [7] [8]. The scope of this study is to examine the oil flow characteristics at a chosen sensor location in the engine and investigate the presence and character of aeration that could potentially influence the measurements of permittivity. Such studies will lay the foundation for proper assessment of engine oil quality and pave the way for the potential application of sensor-based machine learning algorithms for *in situ* engine health monitoring [9] [10] [11] [12].

While aeration in lubricating oil can appear as dissolved air, entrapped bubbles, and surface foam, this study primarily examines entrapped bubbles, as they can potentially influence permittivity-based oil quality sensing. The main source of entrapped bubbles in engines is droplet and jet impact during oil drain-back to the sump [13] [14]. The presence of a baffle plate in the oil sump has been shown to minimize aeration to less than 1% by volume but not completely eliminate it [15].

Engine oil aeration has been previously examined primarily using two techniques: flow visualization and X-ray density measurements. In the flow visualization context, engines have been modified by installing optical windows in various locations on the engine block to capture images of lubricant flow for qualitative and quantitative assessment [13] [16] [17]. Cheng et. al. used an x-ray apparatus to estimate a circulating lubricant's aeration by measuring the difference in density between non-aerated and aerated oil [18] [19]. While all these studies have pointed to the presence of aeration, the results vary dramatically depending on the location at which oil is examined, with measured aeration rates varying between 1%-15% [15].

The purpose of this study is to examine the flow characteristics at a chosen sensor location on an engine requiring no modification to the engine block. Before placement of a permittivity-based sensor for *in situ* oil quality assessment, it would be essential to examine the aeration characteristics of the oil flow.

2.2 Experiment Design

2.2.1 Testbed Diesel Engine Facility

The engine testbed used in the current study (Figure 2.1) consists of a Volkswagen 4-cylinder, 1.9L TDI engine attached to a controllable KLAM K40 eddy-current dynamometer to provide a brake load to the engine. This setup can produce a maximum power of 44 kW at 3600 rpm. The test facility is user-controlled through a computer interface, and the instrumentation data can be accessed through on-board diagnostics (OBD) software. All tests in the flow visualization studies were conducted using clean Shell Rotella T6 5W-40 oil, one of the specified lubricants for the engine.

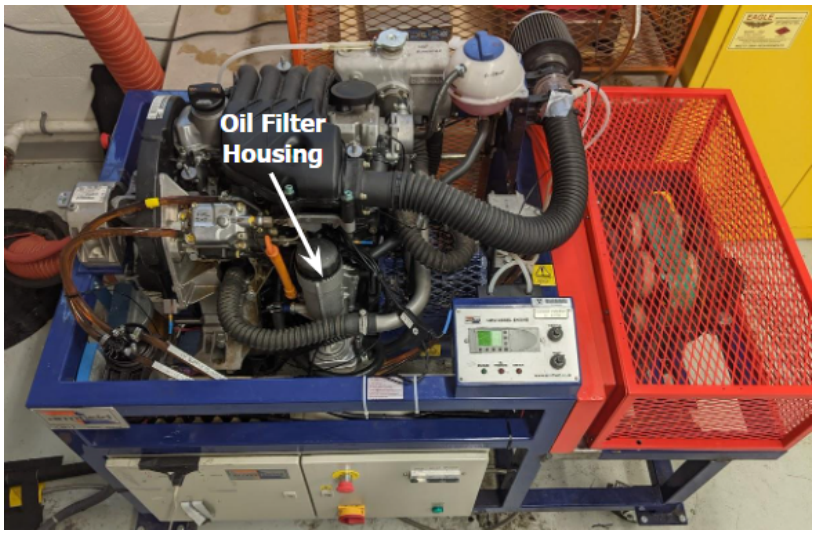

Figure 2.1: Volkswagen 4-cylinder, 1.9L TDI testbed engine facility with dynamometer.

2.2.2 Flow Cell Design and Evaluation

The body of the oil filter housing shown in Figure 2.2 was identified as an accessible location where the oil flow can be continuously sampled by the oil quality sensor without making modifications to the engine block. To optically examine the flow characteristics, oil is extracted prior to reaching the filter by modifying the oil filter housing complex through the addition of a flow diverter prior to the oil cooler. The flow is passed through an external flow visualization cell and returned back to the oil cooler with minimal addition of path resistance. The design of this visualization cell was tested in a benchtop facility at typical engine flow conditions prior to implementation on the engine. The benchtop facility has been specifically designed to emulate engine operating conditions [20].

The flow visualization cell (Figure 2.4) was connected to the filter housing using Parker series 201 hoses rated for engine operating pressures and temperatures with the appropriate adapters. The windows in the flow cell are solid polycarbonate, pressure-sealed to the body of the cell with silicone gaskets. The oil filter

housing assembly with the flow diverter is shown in Figure 2.3, and the full benchtop flow visualization test assembly is shown in Figure 2.5.

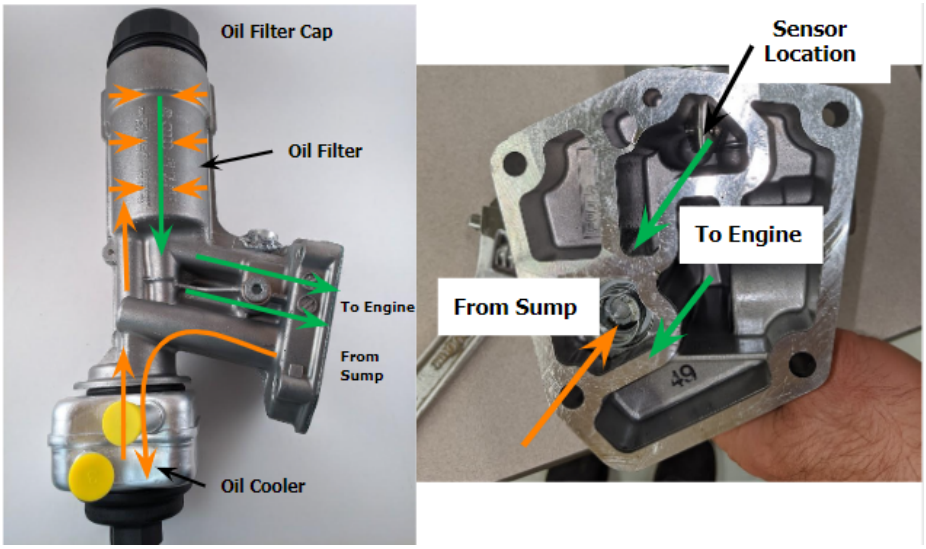

Figure 2.2: Flow schematic of the stock Volkswagen 1.9L TDI oil filter housing, where orange arrows represent pre-filter flow and green arrows represent post-filter flow.

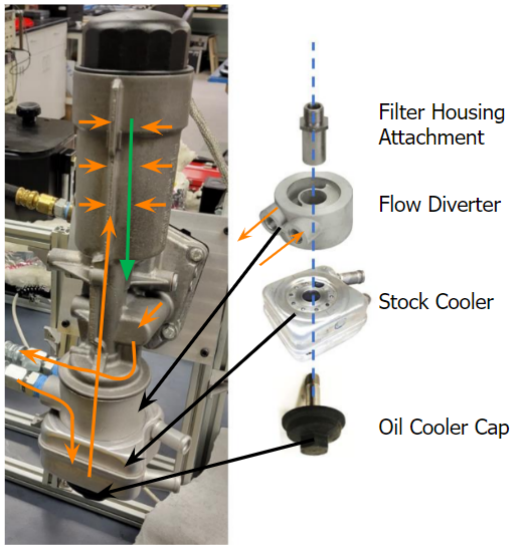

Figure 2.3: Oil filter housing assembly with the flow diverter integrated in the pre-filter oil flow line.

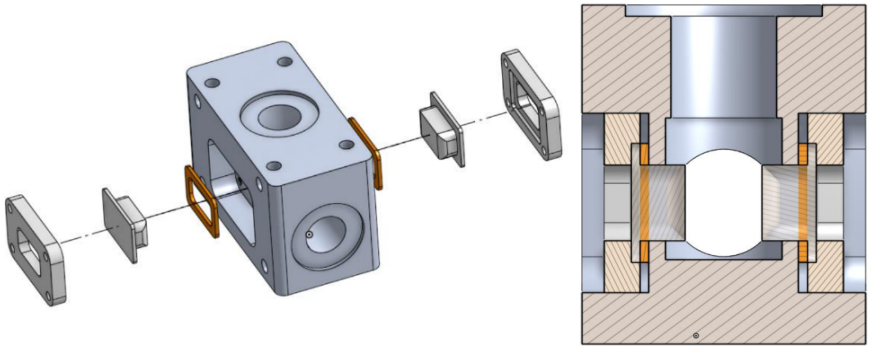

Figure 2.4: CAD rendering of the flow visualization cell.

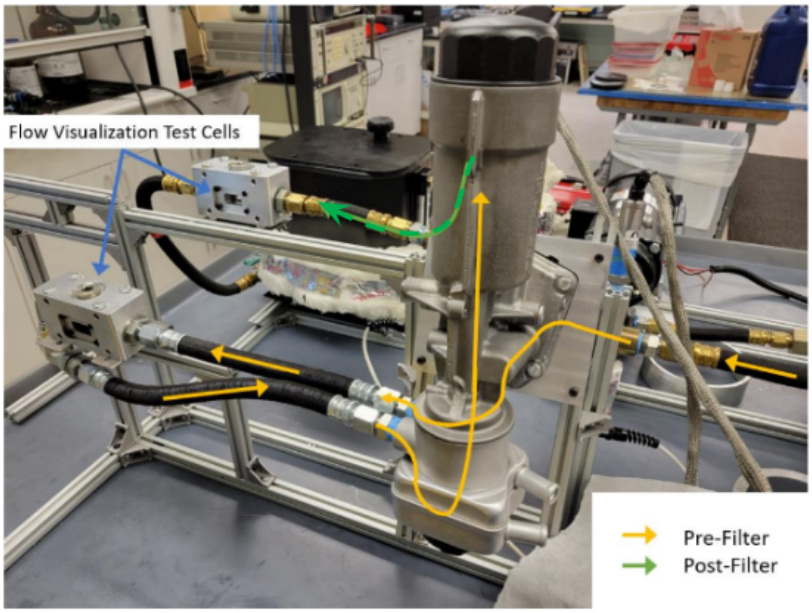

Figure 2.5: Oil filter housing and flow visualization test cells incorporated onto the benchtop test facility. The facility is capable of emulating engine operating conditions in a controllable manner. Oil flow temperature is monitored at the entrance and exit of the filter.

2.2.3 Imaging System and Image Processing Technique

To image the oil flow, a backlighting approach was used so that the silhouettes of any bubbles would be captured by a camera with a shallow depth of field. For this purpose, a Chronos 1.4 high-speed color camera (1280x1024 pixel resolution) with variable exposure time was used, and a 100W white LED light provided continuous backlighting. Additionally, to obtain high-clarity still images for post-processing, a 3 µs-duration pulsed strobe backlight (GenRad 1538 strobe) was used in conjunction with the open-gated video camera operating at 30 fps. The camera's depth of field with its 55mm MicroNikkor lens and 2x magnifier and a fully open aperture was calibrated to be 1.0 mm. The camera's imaging field of view was 7.5mm by 6.0mm.

A schematic of the imaging setup is shown in Figure 2.6.

The *ImageJ* image processing software was used to analyze the images. To estimate volumetric aeration percentage, a threshold was applied to the images to produce a binary black-and-white image in which the bubbles were isolated from the background. The "Particle Analysis" feature of the software was used along with a circularity threshold and size threshold to isolate the in-focus bubbles for analysis and ensure the results were not biased by any dark spots or streaks not removed in the initial thresholding. The diameter of individual bubbles was measurable to a precision of ± 8 µm. An example of the thresholding sequence is shown in Figure 2.7.

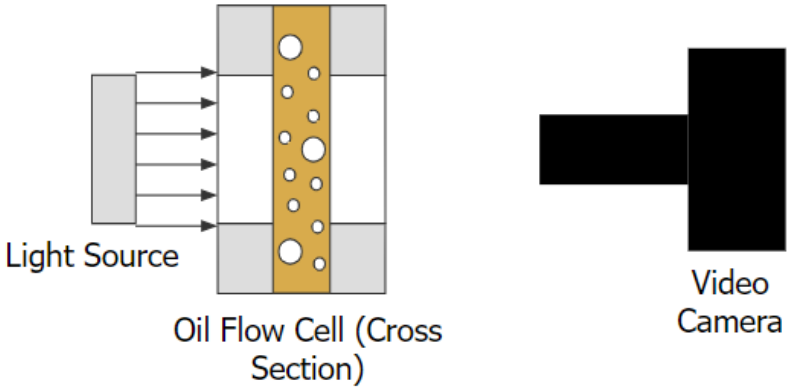

Figure 2.6: Top-down schematic of the backlit imaging setup.

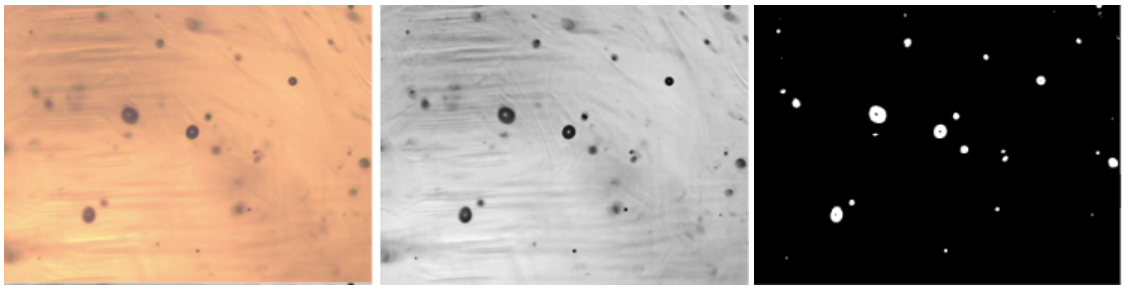

Figure 2.7: Thresholding sequence of strobe-generated bubble silhouettes in moving oil. (L-R) Raw image, grayscale image, thresholded binary image.

2.2.4 Flow Cell Implementation at the Engine

After benchtop validation, the flow visualization facility was integrated into the engine testbed as shown in Figure 2.8. Before setting up for the experiments with clean engine oil, the existing engine oil was drained, and the engine was flushed twice with clean oil. A sample of clean oil was then loaded into the engine to the recommended level on the dipstick.

During the experiments, once the engine was started, it was set to a constant throttle and brake load

and allowed to thermally equilibrate, which typically took twenty minutes (Figure 2.9). The engine oil temperature was measured by the thermistor on an oil quality sensor implemented downstream of the filter. Engine coolant temperature was also monitored using the engine's OBD suite; however, notably, the coolant temperature does not track the oil temperature, which is a required parameter for this study. Imaging was initiated once equilibrium was reached, and during the imaging period, the temperature of the oil held steady to within a precision of $\pm$ 2°F. Typically, several two-second video clips were taken at 1000 fps with 20 µs exposure time for flow speed analysis. Additionally, the continuous backlight was substituted with strobe lighting to capture video photographs (30 fps) with minimal motion blur for better analysis of bubble size. This visualization protocol was repeated for several different engine speeds and oil equilibrium temperatures by adjusting the engine power setting.

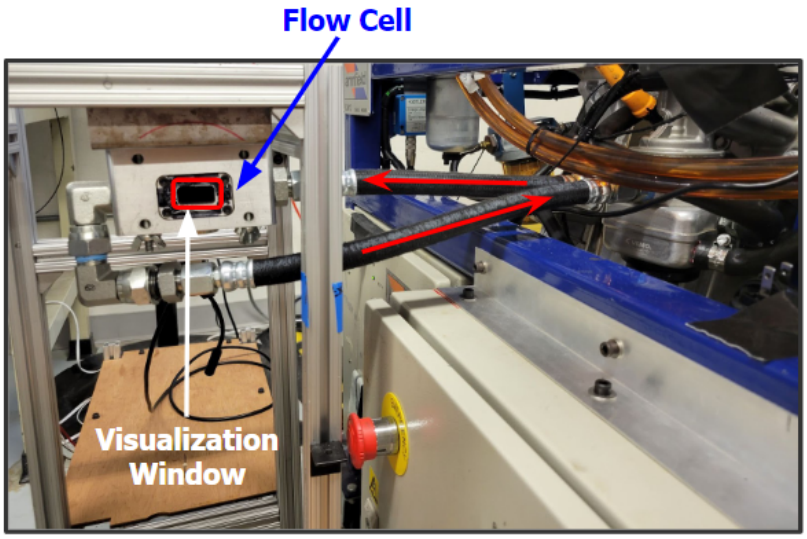

Figure 2.8: External flow visualization facility integrated into the engine testbed.

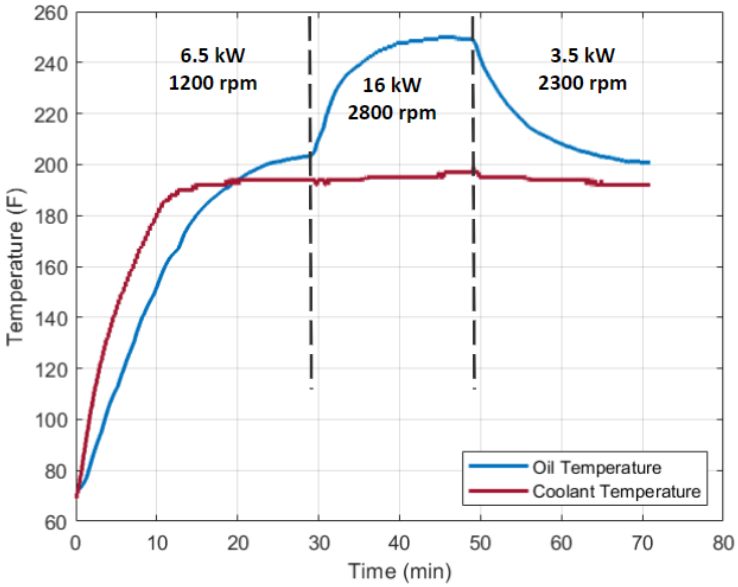

Figure 2.9: Temperature data collected during a typical engine run. The engine brake powers and speeds during operation are denoted.

2.3 Flow Visualization Results

To estimate the approximate flow speed of the engine lubricant through the channel, high-speed footage was used in conjunction with image processing to track individual bubbles. Sequences of images in which a pair of bubbles were in focus and moving in a straight line parallel to the flow were analyzed. The sequence shown in Figure 2.10 was taken from footage at an engine speed of 2800 rpm and oil temperature of 224°F.

The bubble at the top of the images in Figure 2.10 moved at an average speed of 1.3 m/s, and the bubble at the bottom moved at an average speed of 2.0 m/s. Assuming the oil flow in the channel to be laminar, a parabolic flow velocity profile was fitted using the bubble speeds and known separation distance between the bubbles to numerically solve for the centerline velocity and corresponding radial location (equation 2.1):

$$u_i = \frac{u_c}{2}(1 - \frac{r_i^2}{r^2}) \tag{2.1}$$

where r is the equivalent radius of the flow passage, r_i is the distance of a bubble from the centerline and u_i its velocity, and u_c is the centerline velocity. The resulting parabolic flow profile, with an average velocity of approximately 1.1 m/s, is shown in Figure 2.11.

The working oil's kinematic viscosity at 224°F is around 12.9 cSt as interpreted using Walther's equation and manufacturer provided data [20]. The diameter of the flow channel through which the bubbles were imaged was 17.3 mm. These parameters result in a flow Reynolds number of around 1500, verifying that the flow in the channel is laminar.

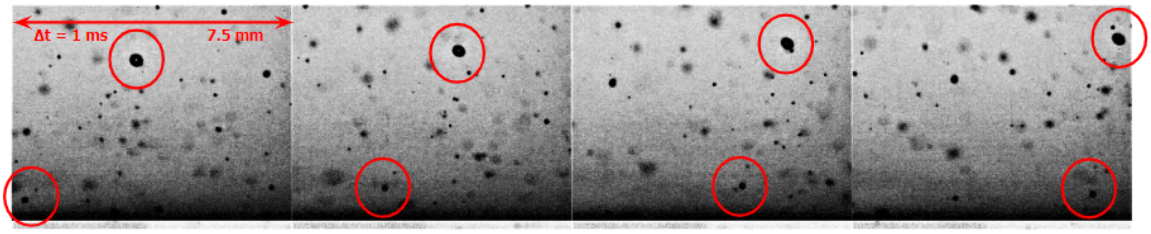

Figure 2.10: Typical flow image sequence at 1000 fps, with the engine operating at 2800 rpm and an oil temperature of 224°F. Bubbles used to model flow velocity (Figure 2.11) are highlighted with red circles.

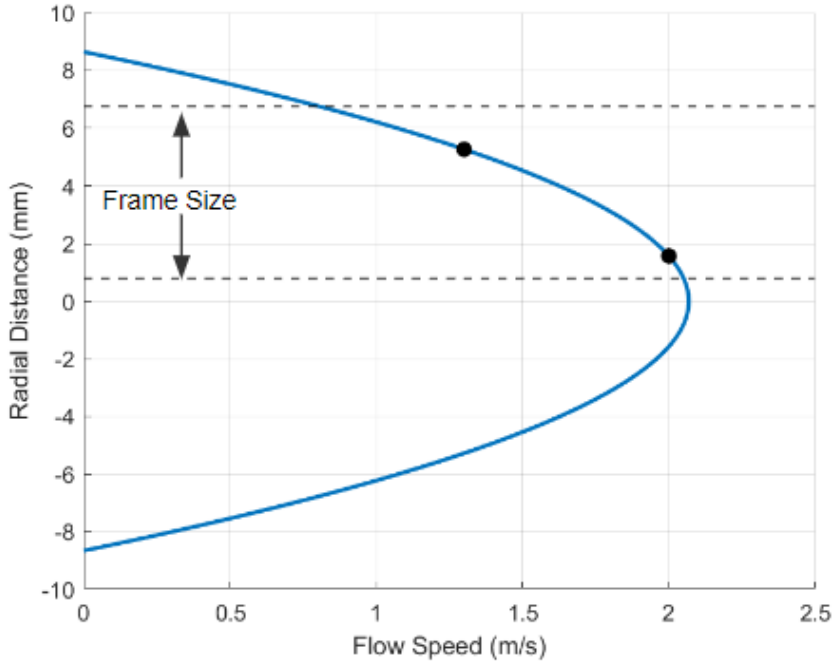

Figure 2.11: Laminar velocity profile model of the oil flow in the test cell. Points indicate data from image sequence shown in Figure 2.10.

Having validated the flow field analysis scheme, this procedure was implemented several times to examine the trajectories of other bubble pairs (Figure 2.12), the results of which are shown in Figure 2.13. The average volumetric flow rate through the channel was estimated to be 3.5 ± 0.5 gpm. The uncertainty of this measurement can be attributed primarily to the use of bubbles as flow tracers and the assumption that they are in equilibrium with the flow [21]. Additionally, minor changes in the flow geometry at the test cell could also contribute to this uncertainty.

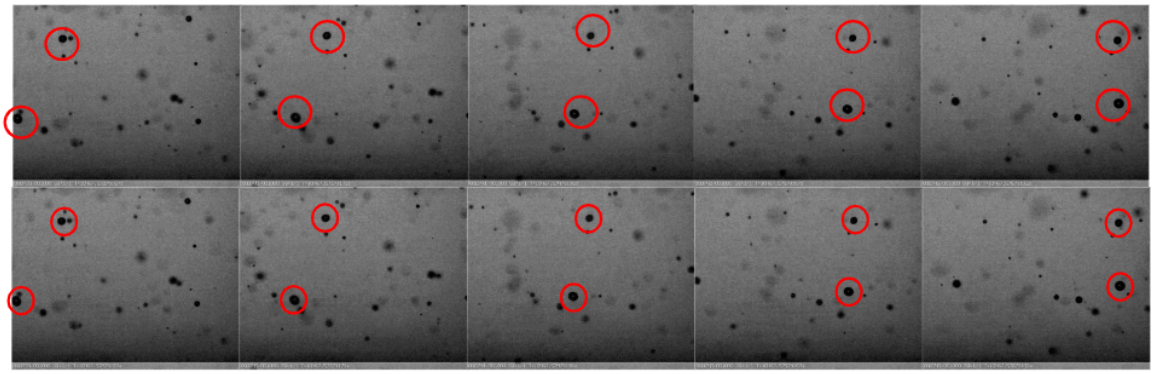

Figure 2.12: Additional image sequences tracking bubble pairs for flow speed analysis in Figure 2.13.

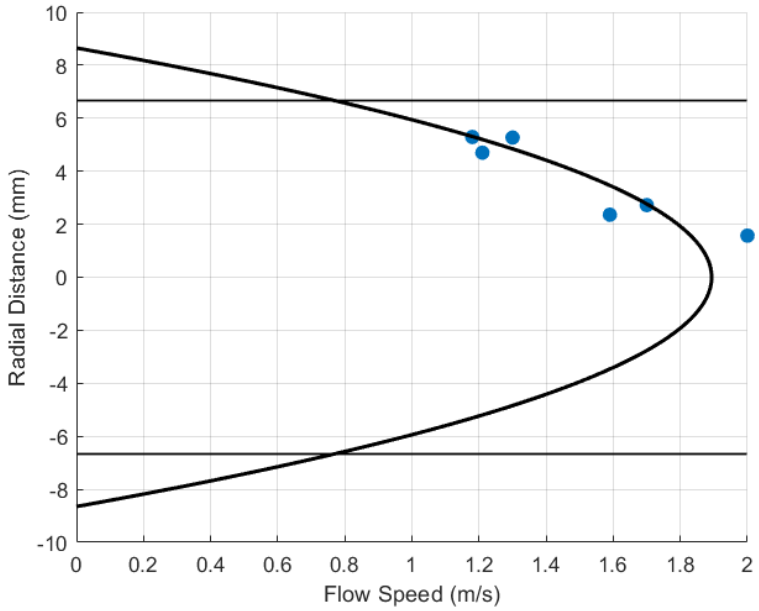

Figure 2.13: Average flow profile using data obtained from image sequences in Figures 2.10 and 2.12.

Bubble number density was established for a sample of a thousand randomly selected strobe-imaged bubbles for the engine run conditions of 2800 rpm and 224°F, and the results are shown in Figure 2.14. Based on the histogram, a log-normal distribution was fit to the data, and the peak in the number density was established to be around 60 µm in diameter. Representative strobe-lit images used in the data analysis are shown in Figure 2.15. The flow field was additionally probed using a high-magnification ($\sim$2 µm/pixel) microscope camera (DinoLite) in conjunction with the strobe lighting to verify the absence of any smaller bubbles ($<$ 15 µm).

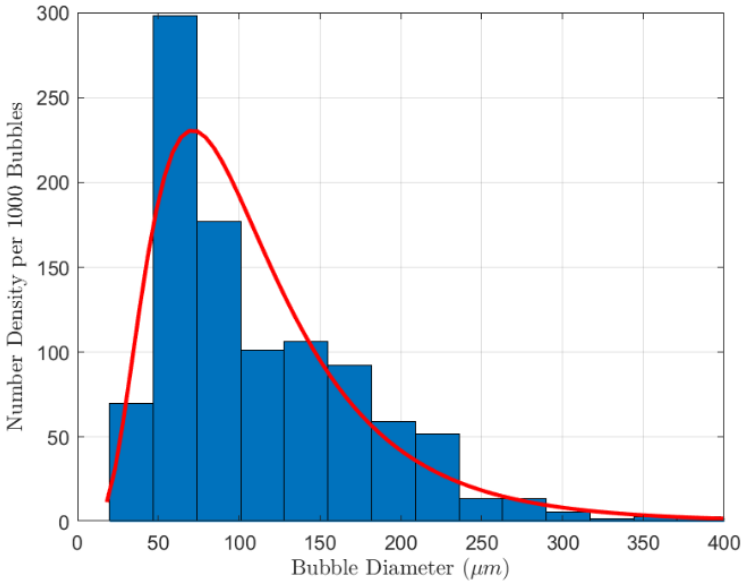

Figure 2.14: Bubble number density histogram showing a log-normal distribution for typical engine operating conditions of 2800 rpm, 224°F.

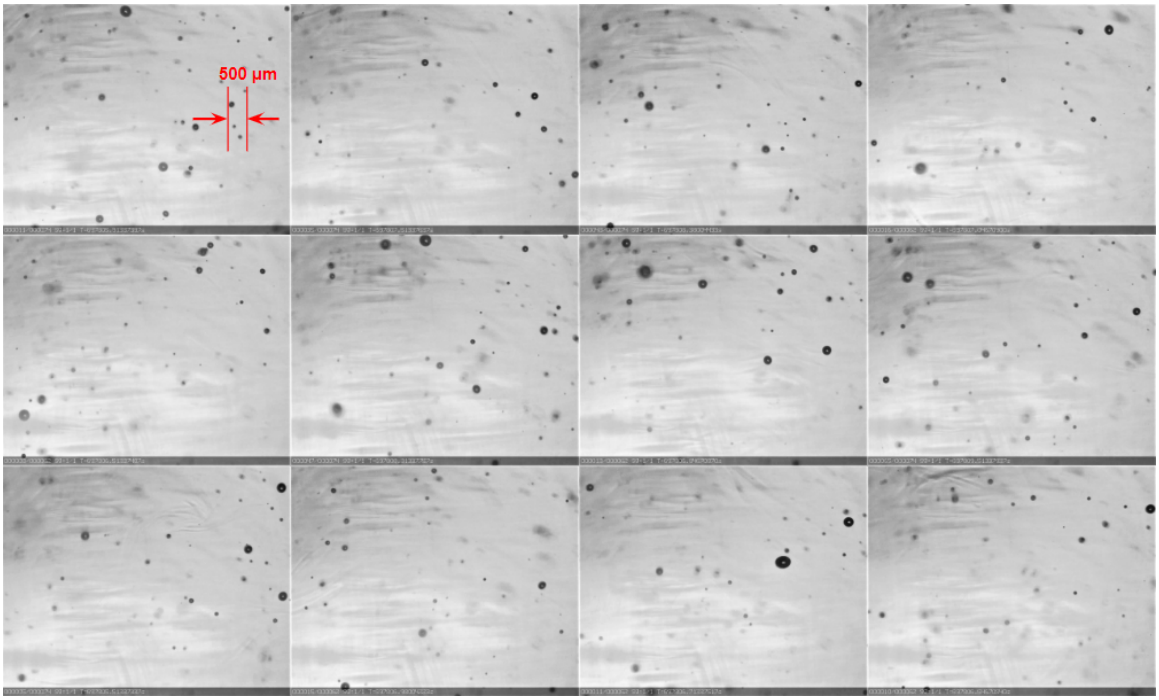

Figure 2.15: Sample of images used to obtain bubble number distribution in flowing oil at an engine speed of 2800 rpm and 224°F.

Volumetric aeration percentage in the flow field was estimated by establishing the size of bubbles in a picture frame with a measured depth of field. Imaging was done at three different engine speeds: 1500, 2200, and 2800 rpm, with the temperature of the oil holding steady at 220 $\pm$ 5°F. Additionally, during engine warm-

up and quasi-steady equilibrium at a fixed engine speed of 2800 rpm, images were taken at three different temperatures: 165 $\pm$ 5°F, 195 $\pm$ 5°F, and 225 $\pm$ 5°F. Ten pictures were analyzed at each set of working parameters to obtain an aggregate estimate of the volumetric aeration percentage. Figure 2.16 captures the effect of viscosity, showing a decrease in bubble size with increasing temperature. The data in Figure 2.17 shows the variation of aeration percentage with temperature and engine speed, with aeration increasing with engine speed and decreasing with temperature. Since volumetric aeration estimation includes bubbles of a spectrum of sizes with larger bubbles contributing to aeration more than smaller bubbles, the uncertainty in aeration estimation resulting from bubble size uncertainty would be relatively low (less than 10%).

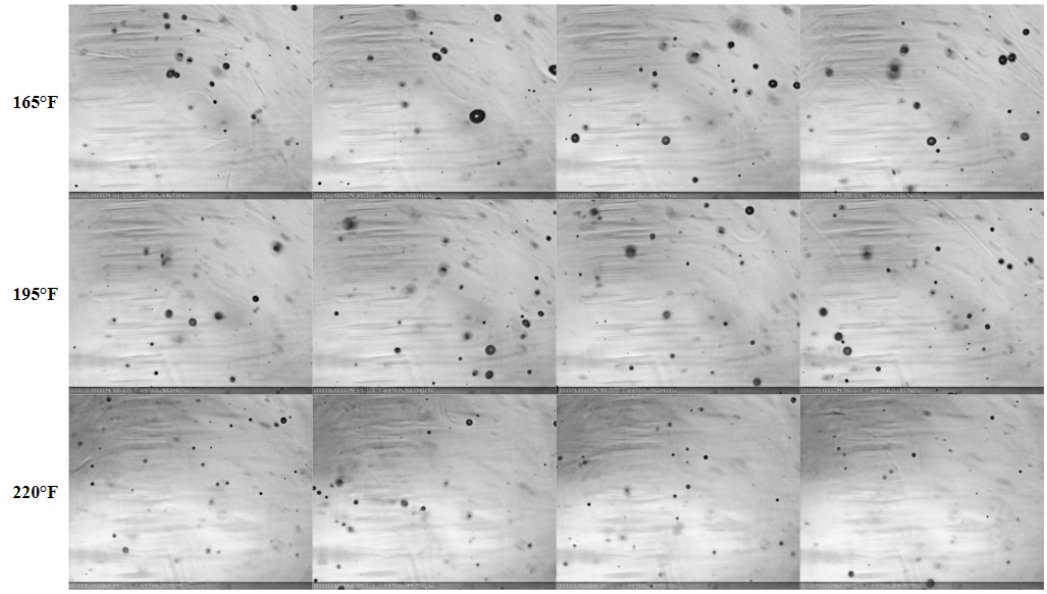

Figure 2.16: Sample images taken at an engine speed of 2800 rpm at three different temperatures.

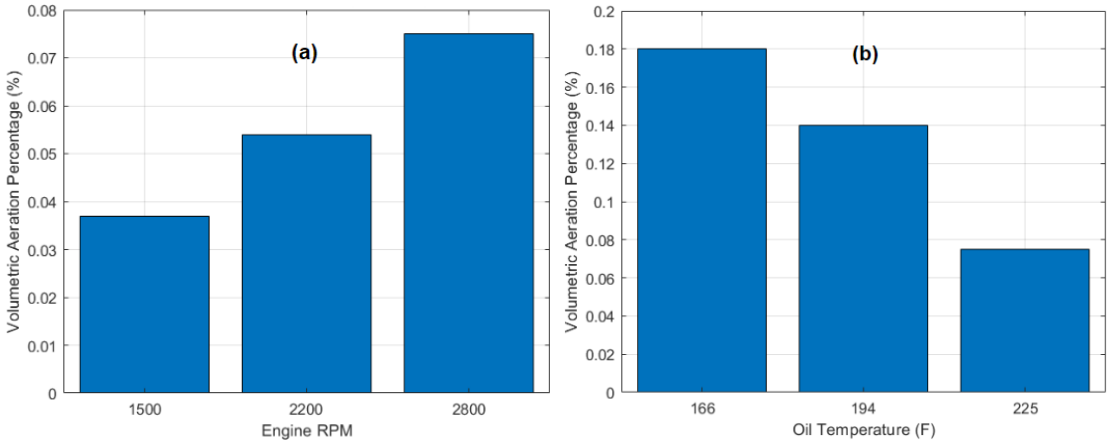

Figure 2.17: (a) Variation of volumetric aeration percentage with engine speed at constant temperature (220 $\pm$ 5°F). (b) Variation of volumetric aeration percentage with oil temperature at constant engine speed (2800 rpm).

2.4 Interpretation of Flow Characteristics

During the oil drain-back to the sump, oil droplets and jets are constantly entrapping bubbles [14] as they impact the free oil surface (Figure 2.18). Whether these bubbles stay entrained in the oil or rise out due to buoyancy depends on the viscosity of the oil and the residence time of the oil in the sump. The competition between buoyancy and pump suction influences bubble size and number density.

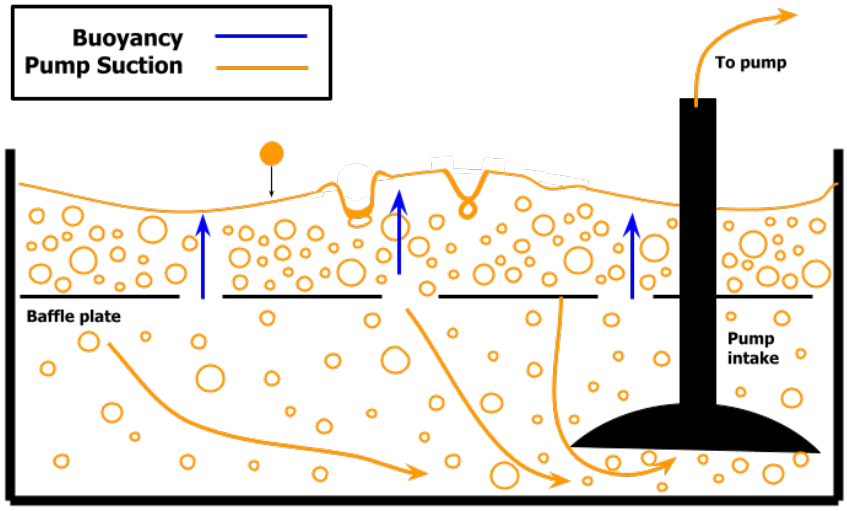

Figure 2.18: Engine oil sump environment during engine operation.

Decreased residence time of oil in the sump leads to increased aeration, as more bubbles become trapped in the oil flow. As engine speed increases at a constant temperature, the aeration increases due to the direct coupling between the oil pump and the engine (Figure 2.17a). Oil temperature affects aeration primarily through viscosity change. When the lubricant temperature is lower (during engine warm up), its viscosity is much higher, bigger bubbles are trapped in the flow, and volumetric aeration is higher. Figure 2.17b shows the results of a constant engine speed run with the oil at various working temperatures.

Engine lubricants also contain anti-foam additives that improve lubrication effectiveness by reducing the oil's surface tension. As shown by Deng et. al. [14], who examined bubble entrapment during droplet impact, a reduction in the oil's surface tension leads to a reduction in the size of bubbles entrapped by droplet impact. Thereby, anti-foam additives lead to lowering of volumetric aeration percentage, with the effect weakening as a degrading oil's additives become depleted with engine use. In addition, the viscosity of a working oil increases with use; this effect has been studied extensively through laboratory testing [6] [22] [23]. Higher oil viscosity results in higher aeration percentages, as demonstrated by the current studies (Figure 2.17b). However, the current visualization studies could not be extended to used/degraded oils due to their extreme opacity. Interrogation of such oils could require other sensing techniques like x-rays, infrared, and ultrasound [18] [19] [24] [25].

CHAPTER 3

Evaluation of Oil Quality Sensor (OQS) in the Benchtop Flow Facility

3.1 Background

Oil quality assessment is very important for the effective functioning of marine and land-based engines used for power production. In conventional automobiles, mileage can be used as an approximate analog to quantify oil degradation, but in other applications such as diesel generators and marine engines, no such acceptable metric exists because in these contexts, engine operating time, loading, and oil quality have not been well-correlated. In a typical ship diesel engine, lubricating oil samples are taken periodically and laboratory tested to determine their degradation level [11] [12], but this process is not an effective universal solution. *In situ* oil quality assessment would be beneficial in all such situations. Successful implementation of oil quality sensors requires an understanding of the oil flow at the chosen sensor location in the engine with the sensor placement preferably requiring no modification to the engine block. The current work identifies a post-filter-flow location on the oil filter housing as a suitable location where the response of a commercial off-the-shelf (COTS) permittivity-based oil quality sensor (TanDelta OQS GenII) has been assessed under several different engine operating conditions.

The TanDelta OQS deployed in this study uses complex permittivity measurements to estimate the operational quality of a lubricating oil. Electrical permittivity, and its associated loss factor, change due to oxidative degeneration of oil with use [7] [8] [26] [27]. The cylindrical capacitor that makes up the sensing element of the OQS allows oil to continuously flow through the capacitor gap (Figure 3.1), where the dielectric assessment of the oil is made. The sensor applies a high frequency alternating current across the electrodes to determine the capacitance and conductance of the dielectric material. In general, as a lubricating oil deteriorates, the proportion of polar molecules in the oil increases and thereby the electrical conductivity of the dielectric medium increases [7] [8] [26] [27]. Because this assessment is done using a very high frequency (MHz) alternating current, there is no translational mobility of the polar molecules; instead, there is only a locational assessment of conductivity which results in a local loss of energy. The permittivity of the dielectric is expressed as a complex permittivity, consisting of an energy storage term (capacitance) and a loss term (conductance); the ratio between these two terms is known as the "tan(δ)" (tangent delta). Studies have shown that the energy storage capability (capacitance) of the oil does not change appreciably with oil degradation compared to the polar molecule-based energy loss property (conductivity) [8] [26].

The OQS reports the tanδ measurement as a loss factor percentage using a proprietary algorithm devel-

oped by the manufacturer to consistently represent oil quality for any chosen oil. Specific oils are degraded using oxidation catalysts, and a unique map between tanδ measurements and loss factor percentage is developed for each oil. At engine operating temperatures, a loss factor percentage range of approximately -4 LF% to 6 LF% represents the spectrum of clean to functionally good oil, whereas 6 LF% to 25 LF% represents various levels of deteriorated oil.

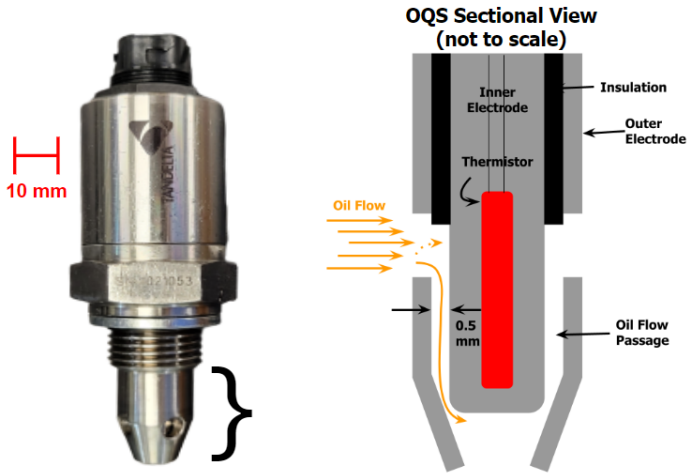

Figure 3.1: TanDelta Oil Quality Sensor (OQS) and schematic of sensing tip.

Basu et. al. have previously developed a smart sensor which measures the electrical conductivity of an oil, interrogated at low frequencies, and correlated the measurements to chemical properties such as total acid number (TAN) and total base number (TBN) [28]. Preliminary *in situ* engine oil quality measurements have been explored by Clark and Fajardo [29], who implemented a multi-functional sensor capable of measuring dielectric constant, viscosity, density, and temperature in diesel engine lubricant flow. Their results showed that viscosity of the lubricating oil increases and the dielectric constant decreases with oil degradation, pointing out that such sensing is feasible. Byington et. al. field-tested an on-line OQS on diesel army vehicles to estimate lubricant oil life and found the preliminary results promising [30].

The current study systematically examines the performance of a COTS oil quality sensor implemented in a chosen flow-field location on a diesel engine and determines its applicability for real-time sensing in the context of engine health management. The goal of these studies is not to run an engine continuously for several hundred hours to reach advanced stages of oil deterioration but rather to focus on the compositional aspects of the flow field in the engine which could influence permittivity-based measurements.

3.2 Benchtop Facility and Experimental Procedure

Figure 3.1 shows the oil quality sensor (TanDelta OQS GenII) that was tested on a benchtop test facility and then implemented on the diesel engine testbed. It has circumferential ports that facilitate continuous flushing

of the sampling region, which is about 0.5 mm wide. The interrogation frequency of the sensor is in the megahertz regime, but the sensor reports an averaged reading of samples at around 1 Hz to eliminate the transient effects of any flow-field inclusions that might bias measurements.

The focus of the current study is to examine the effect of aeration in the engine flow field [15] on sensor loss factor measurement. Air and oil have drastically different dielectric properties [31] [32], and despite averaging, the effect of the constant presence of air in the working fluid will deliver a lower loss factor (higher quality) assessment of the oil [33] [34]. This biasing effect must be well understood before incorporating oil quality sensors for *in situ* measurement, especially in the context of the design of expert systems that might use machine learning algorithms to assess engine health and recommend oil changes.

A benchtop test facility was designed to conduct parametric evaluation of the OQS under controlled conditions, emulating those found in the engine described in Section 2.2.1 [20]. Whereas on the engine, oil flow parameters such as temperature and flow rate cannot be directly controlled, the benchtop facility can replicate the engine equilibrium temperatures and flow conditions in a controlled manner. In addition, the benchtop provides the capability to examine the spatial orientation of the sensor and its effects on measurement. While the benchtop facility emulates engine oil flow conditions, it does not contribute to further oil degradation during testing, and guarantees non-aerated flow during operation.

In the benchtop, the oil flow is circulated through an oil filter housing identical to that on the engine. The facility has been designed for 80 psi operating pressure, a maximum fluid temperature of 250°F, and a flow rate between 2 gpm and 6 gpm, emulating most of the engine operating conditions. In the test protocols used in this study, oil is first run on the engine then extracted to be tested on the benchtop facility. Normally, the testbed engine runs on 4-4.5 quarts of oil, but since the extraction volume from an engine is generally lower than its full capacity, the benchtop facility has been designed to operate with a minimum of 3 quarts of oil.

The facility has inline calibrated pressure and temperature sensors and a flow meter. The temperature of the oil is controllable to ± 0.6°C (± 1°F), the flow rate is controllable to ± 0.19 L/min (± 0.05 gpm), and the pressure is measured to ± 0.7 kPa (± 0.1 psi). Since the overall flow surface area in the facility is relatively low compared to that of the engine, more than 95% of the mass of its working fluid can be recovered when draining. Flushing protocols further mitigate effects of cross contamination of different oil samples. The facility is shown in Figure 3.2, with major components labeled.

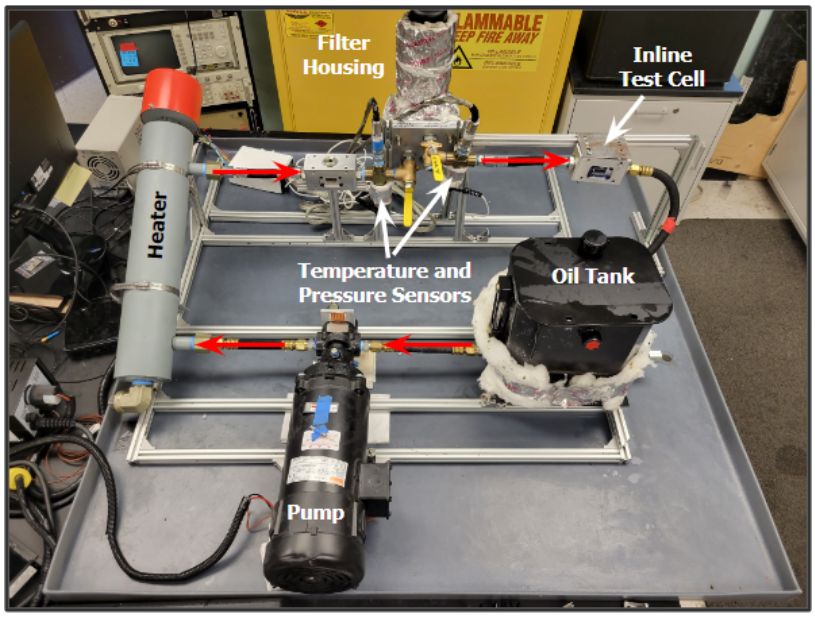

Figure 3.2: Benchtop facility with major components; red arrows show flow direction. Oil quality sensors can be mounted in both inline test cells as well as the filter housing. The flow meter is just upstream of the oil tank and obscured in the picture.

Oil in the benchtop facility is pumped through half-inch hydraulic hoses using a motor-driven positive displacement gear pump. The circulation heater uses a PID-controlled resistive heating element with a large surface area to accurately achieve setpoint temperatures while preventing excess heating and coking. The heater is placed upstream of the filter to guarantee a driving back pressure in the lines to ensure safe and uniform heating. After passing through the heater, the flow is directed past the oil filter complex (shown in detail in Figure 2.2). Volumetric flow rate is assessed using a precision calibrated oval gear flow meter suitable for working temperatures, and the design of the v-gutter in the reservoir ensures that the return flow is smooth and devoid of surface-entrained bubbles.

The filter housing was modified to allow for proper OQS mounting. As shown in Figure 3.2, in the benchtop facility, the oil enters and exits the filter housing through an adapter plate to which the filter housing is mounted. It then moves through an oil cooling heat exchanger, which is functional on the engine but not in this facility, as auxiliary cooling of the oil is unnecessary in a temperature-controlled facility. Access holes were drilled into the oil filter housing, and a threaded adapter piece was welded to mount the OQS such that the sensing element is fully submerged in the post-filter oil flow. Figure 3.3 shows both the horizontal and vertical OQS configurations in the modified oil filter housing.

Oil quality sensors can be positioned both at the filter and at inline-flow test cells, the test cells being installed either upstream or downstream of the filter. The JIC-swivel hoses on the test cells allow for manip-

ulation of the radial position of the OQS to assess the role of sensor orientation in oil quality sensing. At the filter location, the only feasible OQS orientations were horizontal and vertical which were both implemented.

The vertical configuration at the filter required that the sensor be tilted by 15 degrees (Figure 3.6), and it was essential to examine the effect of this tilt, if any, using comparative measurements at the inline test cells. In these studies, two cross-calibrated sensors were used: one at the filter and one inline.

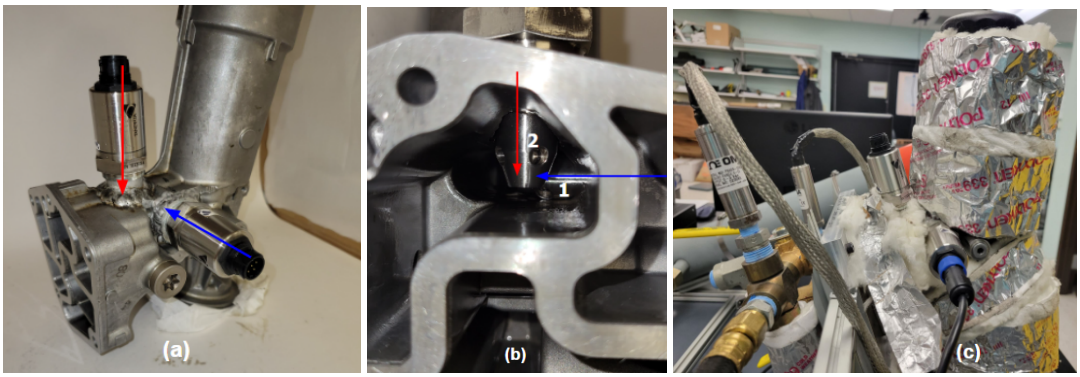

Figure 3.3: Oil quality sensors integrated into the modified oil filter housing. (a) Filter housing OQS orientations. (b) Inside view of sensing elements intercepting the oil flow. (c) Oil filter housing with sensors integrated into benchtop test facility (wrapped with thermal insulation).

The functional operational window of the benchtop facility is shown in Figure 3.4; this was established through a combination of measurements and visual inspection. The maximum operating temperature is 250°F, which is established based on the temperature limits of the pump, flow meter, and sensors. The minimum operating temperature is 90°F and represents the lowest temperature that can be uniformly maintained in the loop. The operational window in Figure 3.4 has been delineated to show the working temperature regime of the engine. The upper flow rate boundary of this window is determined by the pump's maximum power capability (maximum flow rate is dependent on the viscosity of the oil and therefore temperature), and the lower boundary of flow rate is dictated by the requirement to establish a thermally uniform flow.

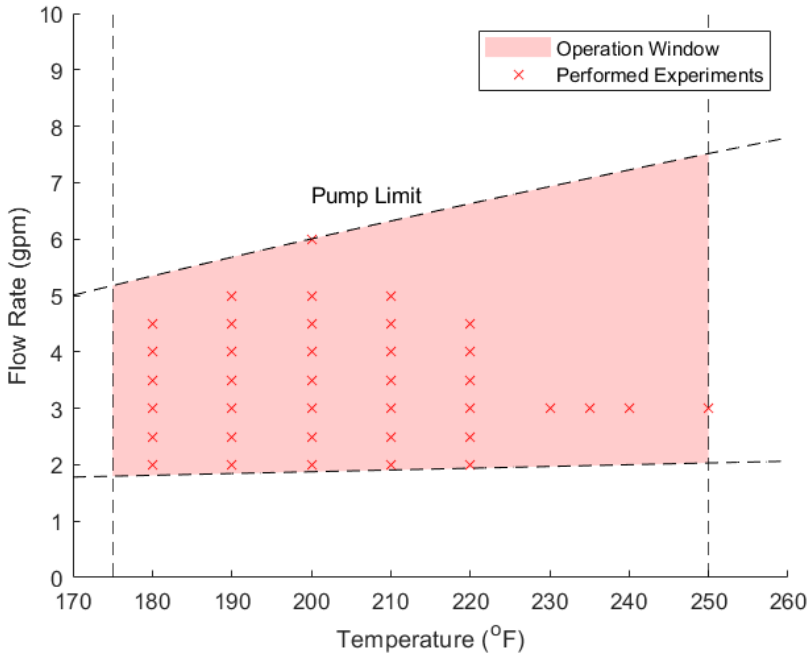

Figure 3.4: Window of operation for the benchtop facility, dictated by operational temperature regime of the engine, pump power limit, and minimum flow speed required for thermal uniformity.

Extensive care was taken to prevent cross-contamination of working samples during the experiments. Between runs, the oil quality sensors were cleaned using the manufacturer recommended procedure; this was especially important to achieve consistent measurements when the facilities were switched from using clean to used oil samples. To prevent different oils from contaminating each other, between runs of different oils, the benchtop facility was flushed twice with a clean sample of the working oil.

Oil samples were always tested first on the engine and then moved to the benchtop to best capture the engine lubricant quality in the benchtop studies and not vice versa. All studies were conducted using the recommended Shell Rotella T6 5W-40 full synthetic motor oil. Three oil samples were tested. Sample A was a fresh oil first used on the engine then tested on the benchtop. Sample B was a used engine oil of the testbed engine that was also tested on the benchtop. Sample C was an oil extracted after 8,300 miles of use from a 2001 Volkswagen Jetta running on an identical TDI engine with 218,000 miles on its odometer. Sample C was only tested on the benchtop facility. After each oil was tested on the benchtop, the facility was flushed twice with clean oil before setting up for a different sample test.

Prior to conducting the experiments, the sensor's baseline loss factor response, with oil quality deterioration, for Shell Rotella T6 5W-40 was established by TanDelta using their proprietary technique. This calibration served as a backdrop for all oil quality assessment studies.

3.3 Oil Quality Sensor Measurement Characteristics

3.3.1 Run-to-Run Measurement Repeatability

Oil sample C was used to verify the repeatability of the loss factor measurements in the benchtop facility with the sensor at the filter location. During the tests, the oil was pumped at 3 gpm, and the temperature was held steady at 220°F for a period of 30 minutes. Loss factor data on the OQS was collected every 3 seconds with the oil temperature measured by the inline pre-filter RTD sensor. Over a thirty-minute run, no variation was noticed outside the sensor's measurement resolution of 0.1 LF%. The aggregate variation over five such runs, each starting with the oil at the baseline room temperature and ramped up to the operating temperature, was verified to be ±0.25 LF% in a previous study performed by Adam Smith [35].

3.3.2 Loss Factor Response to Temperature Change

To understand the OQS's transient and steady state response to stepwise changes in temperature, similar to that which would be expected when changing engine load, oil sample C pumped at 3 gpm was cycled through a temperature ramp up from 140ºF to 220ºF in 10ºF increments as shown in Figure 3.5. The OQS response to a positive temperature slope is an initial drop in loss factor and eventual rise until a steady state value is reached. The response time of the OQS mirrors that of the temperature equilibration time of the facility; this understanding of transient and steady state response is essential when making load changes on the engine and interpreting data. A similar response is recorded when the temperature is ramped down, except that the OQS first shows an increase in loss factor before decreasing to its steady state value. Another aspect to note is that the loss factor progressively increases with temperature, a feature that could represent an increase in the energy loss (conductivity) term of the permittivity measurement.

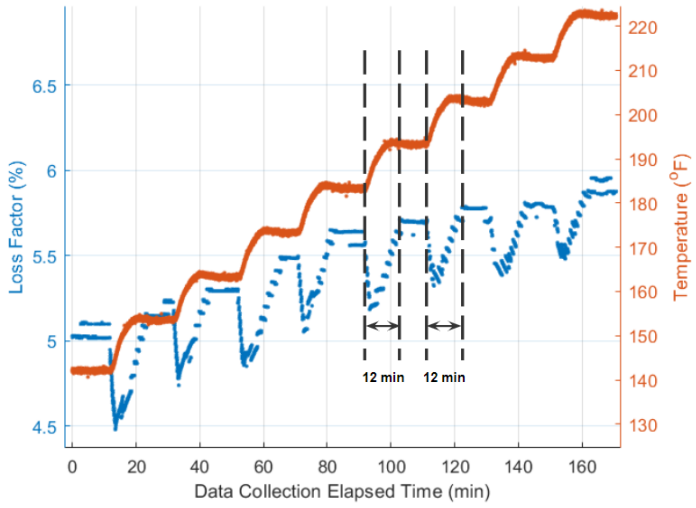

Figure 3.5: Loss factor response to a ramp-up in temperature, with equilibration timescales denoted. Figure from research conducted by Adam Smith [35].

3.3.3 Loss Factor Response to OQS Radial Orientation

The OQS in the engine oil filter housing is angled at 15° from the vertical (Figure 3.6a), as this was the most suitable location to weld the sensor mount onto the filter. To examine the role of orientation and its effects on the loss factor response, tests were conducted to compare OQS measurements at the filter with those of an inline sensor at several radial orientations. These experiments were performed at 220°F and 3.0 gpm flow rate using oil sample C. The inline OQS was oriented at different positions from 0° to 180° in 45° increments (Figure 3.6b).

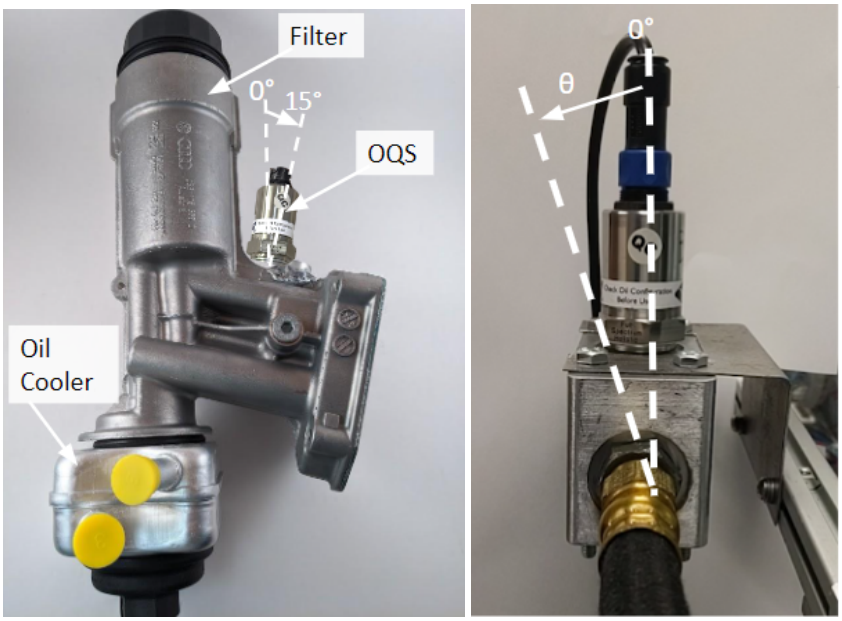

Figure 3.6: (a) OQS as installed on the oil filter housing tilted at 15°. (b) Schematic of the inline OQS, which can be rotated about the hose axis. Figure from research conducted by Adam Smith [35].

The data from these studies is shown in the rose plot in Figure 3.7 from earlier work by Adam Smith [35]. The OQS loss factor response displayed no difference between the vertical and the 15° orientation and was within the standard measurement uncertainty of ±0.25 LF%. The manufacturer recommends that the OQS not be oriented with the sensor facing upwards (135° - 225°) to reduce effects of sediment build-up in long duration, oil-life testing in engines. In the engine implementation studies, the deployed sensor orientations on the filter housing were 15° vertical and 90° horizontal, both of which meet the sensor placement recommendations.

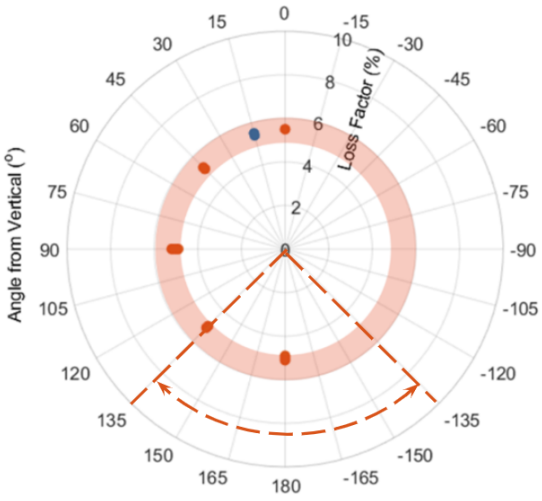

Figure 3.7: Inline OQS loss factor measurements at various orientation angles. The blue dot represents data collected at the filter location (15° from the vertical). Figure from research conducted by Adam Smith [35].

3.3.4 Hysteresis in Loss Factor Response

Figure 3.8 shows the equilibrium loss factor measurements during temperature ramp up and ramp down from tests on oil sample B at a range of steady-state temperatures. One set of data was collected beginning with the oil at an equilibrium temperature of 180°F and increasing the temperature in increments of 10°F to 230°F, and the other set of data was collected beginning at 230°F and decreasing the temperature by 10°F increments to 180°F. During the tests, loss factor measurements were only collected once the oil temperature and loss factor had reached equilibrium at each desired temperature. These tests were conducted to investigate temperature-based hysteresis effects in OQS loss factor measurement at the filter location in the vertical configuration. It was found that the measurements all fell within the sensor's standard uncertainty of ± 0.25 LF%, and no hysteresis effects were detected. These results are important for long-term OQS implementation in engines where repeated thermal cycling is to be expected. Additional tests evaluated the role of lubricant flow rate in the regime of 3-6 gpm at a constant temperature, and no effect on loss factor measurements was found.

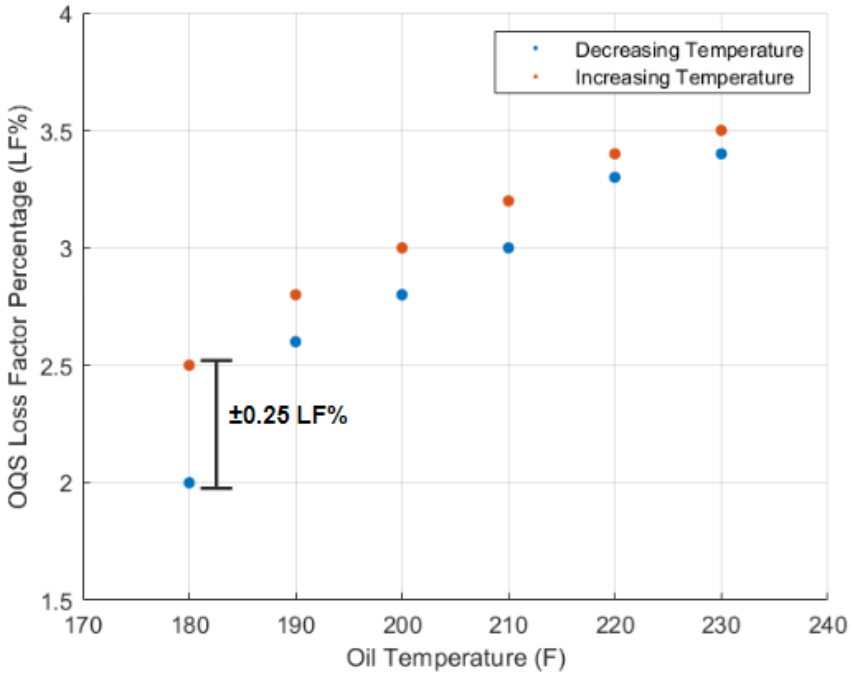

Figure 3.8: Results of temperature-based hysteresis study using oil sample B; measurements taken at the vertical filter location in the benchtop.

CHAPTER 4

Oil Quality Sensor Implementation on the Diesel Engine

4.1 Engine Brake Loading and Test Procedure

Following validation of the modified oil filter housing assembly on the benchtop facility, it was implemented on the testbed engine as shown in Figure 4.1. Figure 4.2 shows the measurements taken during a sample engine test run. The engine was powered up by setting the throttle and resistive brake load to constant values and allowing both the OQS's built-in oil temperature measurement and loss factor measurement to reach equilibrium. After understanding the equilibration times, the engine power (throttle and brake load) was then increased or decreased to achieve a range of oil temperatures. Two pre-cleaned and cross calibrated sensors were used at the filter in both the vertical and horizontal configurations as shown in Figure 3.3a in each of these experiments. It is important to note that the engine experiment protocol mirrored typical load and throttle changes in a power-producing engine, where engine speed is an outcome of the load and throttle changes.

During engine power up, as the temperature rises, the OQS shows the expected response of first decreasing and then increasing to its steady state loss factor value (Figure 4.2). Initially, at engine startup, the sensor sees only air since the oil would have drained back into the sump. Within a few pump cycles, the sensor becomes fully submerged in lubricating oil, from which point, data collection is started. Parametric changes of engine power were initiated after both the OQS temperature and loss factor measurements had reached equilibrium, the timescale of which is on the order of fifteen minutes once the engine has warmed up. In these engine tests, the temperature of the oil is monitored using the built-in RTD thermistor on the OQS. It is important to note that the engine coolant temperature generated from OBD data does not track the oil temperature, as the coolant is actively cooled by the radiator once the thermostat opens.

Engine tests were first conducted with the pre-existing used Shell Rotella T6 5W-40 oil (sample B) in the engine with the OQS mounted at the filter. In all engine tests, before the start of the experiments, the oil level was verified to be in the middle of the range marked on the dipstick.

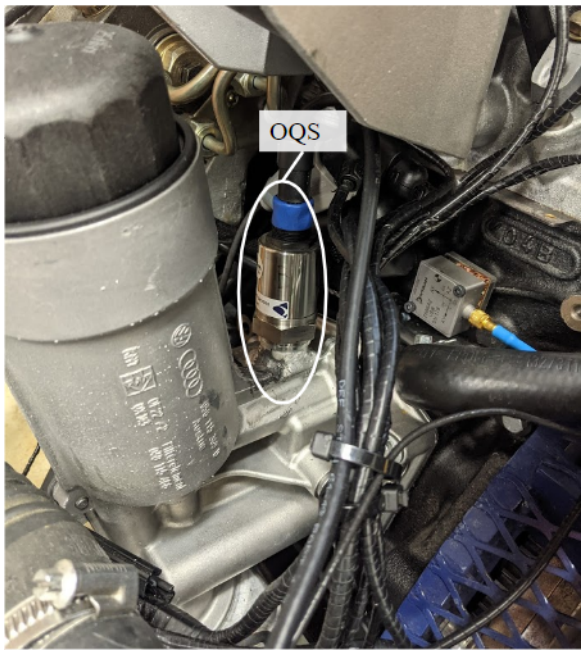

Figure 4.1: Vertical OQS as installed at the oil filter housing on the engine. Oil temperature was monitored by the built-in thermistor on the OQS (Figure 3.1).

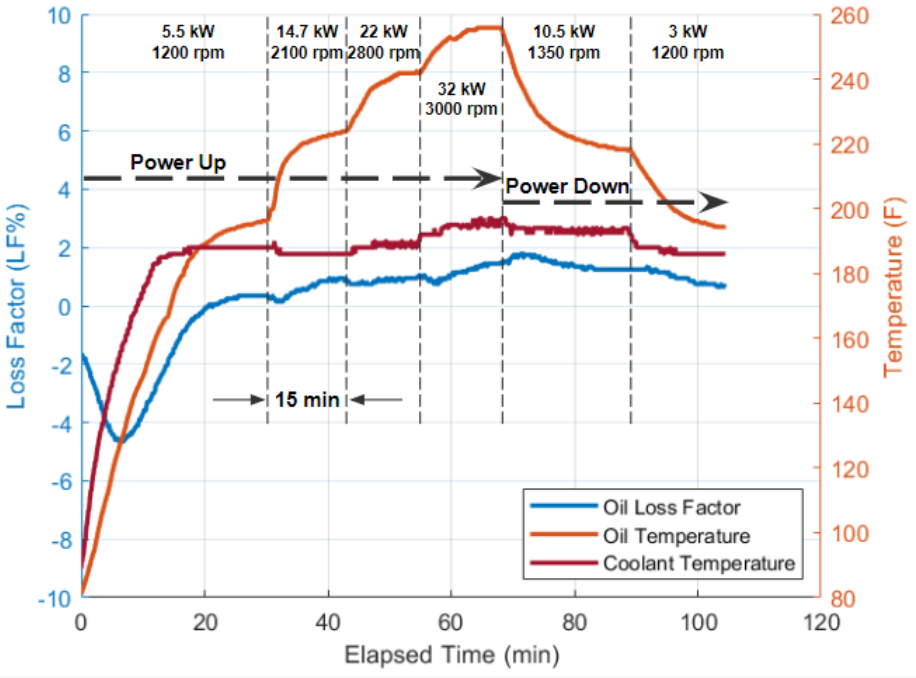

Figure 4.2: Sample measurements from a typical engine test run, showing OQS loss factor, OQS oil temperature, and the engine coolant temperature.

4.2 Oil Quality Sensing Results for Used and Clean Oils

Loss factor data on sample B was collected at engine oil equilibrium temperatures of 195 ± 3°F, 220 ± 3°F, and 240 ± 3°F, corresponding to different engine load and throttle conditions. The testing protocol was repeated after switching the original sensor orientations (vertical to horizontal and vice versa) to examine any measurement bias (of which none was found), and the results of these tests are shown in Figure 4.3. Oil sample B was then drained from the engine and then loaded into the pre-cleaned benchtop facility, and similar tests were performed, the results of which are also shown in Figure 4.3. It is evident from comparing the measurements in the engine and benchtop facility that there is a discrepancy between the measurements in the two facilities, with the engine tests consistently returning lower loss factor values and the difference between the two measurements being larger at lower temperatures. Considering that the benchtop was twice flushed with clean oil before loading the used engine oil (sample B), any dilution effect due to residual clean oil should only make the benchtop measurements lower, not higher, than the engine measurements. The root cause for this difference was investigated further.

Figure 4.3: Comparison of loss factor measurements collected during engine and benchtop tests for oil sample B. Runs 1 and 2 represent horizontal and vertical OQS configurations of the same sensor.

Engine tests were then conducted using a clean sample of Shell Rotella T6 5W-40 (sample A) placed into the pre-flushed engine using the same test protocols as those in Figure 4.2. Sample A was drained from the engine following testing and then tested on the benchtop facility. Again, there is a discrepancy between the two measurements, with the engine returning consistently lower loss factor values with the difference being larger at lower temperatures (Figure 4.4).

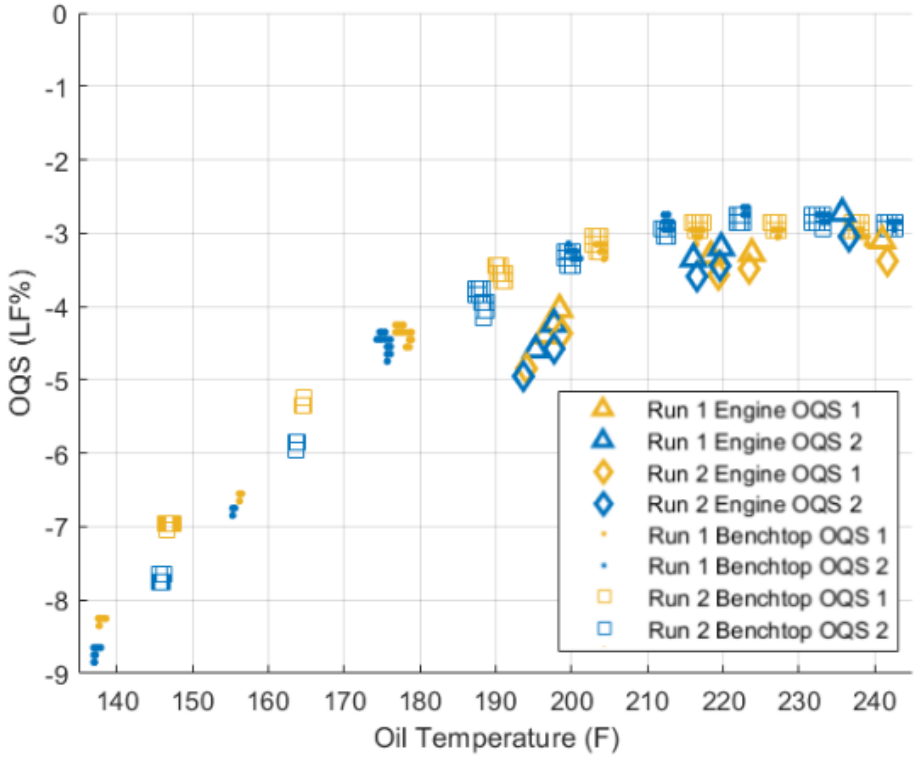

Figure 4.4: Comparison of loss factor measurements from clean oil (sample A) tests on the engine and benchtop.

4.3 Modeling Sensor Response to Temperature in Used and Clean Oils

The permittivity-based loss factor measurements of the sensor at equilibrium conditions show a consistent dependence on temperature both in the engine and benchtop (Figures 4.3 and 4.4). To model this temperature response; an exponential function of the form shown in equation 4.1 was first fit to the data from the controlled benchtop testing with oil sample B, and the resulting fit is shown in Figure 4.5.

$$LF\% = A - \frac{B}{e^{C(\frac{T-T_0}{T_0})}} \tag{4.1}$$

where A, B, and C are fitting constants and T_0 is a reference temperature of 140°F. Figure 4.6 shows single sensor data from the engine and benchtop studies fitted with exponential functions of the form shown in equation 4.1; the difference in the engine and benchtop measurements is captured by these fits.

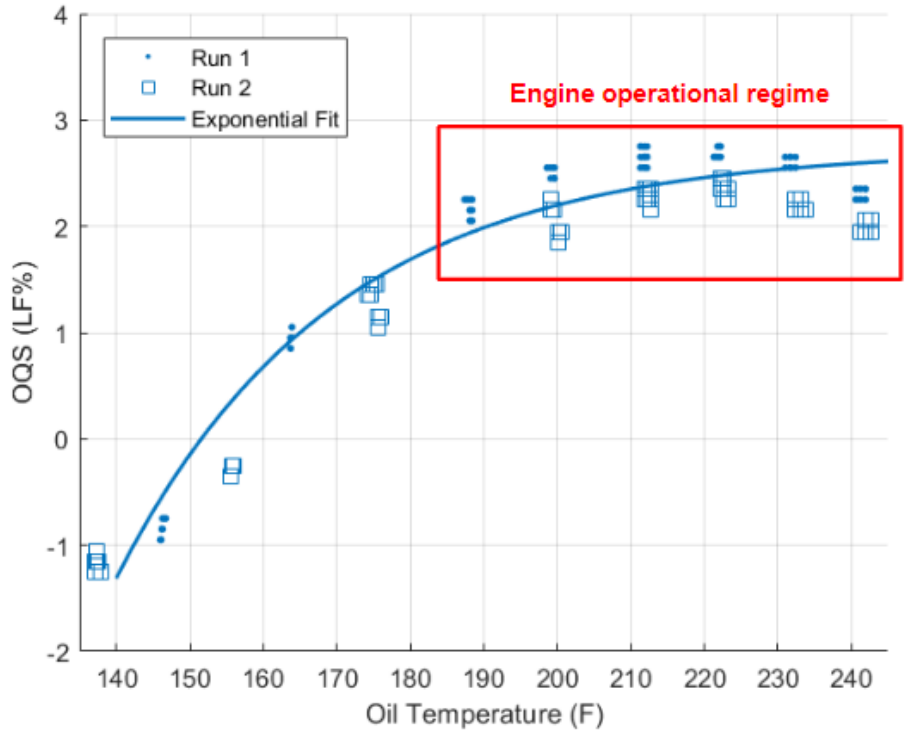

Figure 4.5: Steady state OQS response to temperature in benchtop experiments, fit with exponential function (equation 4.1). The fit constants A, B, and C were approximately 2.2, 3.9, and 4.5, respectively.

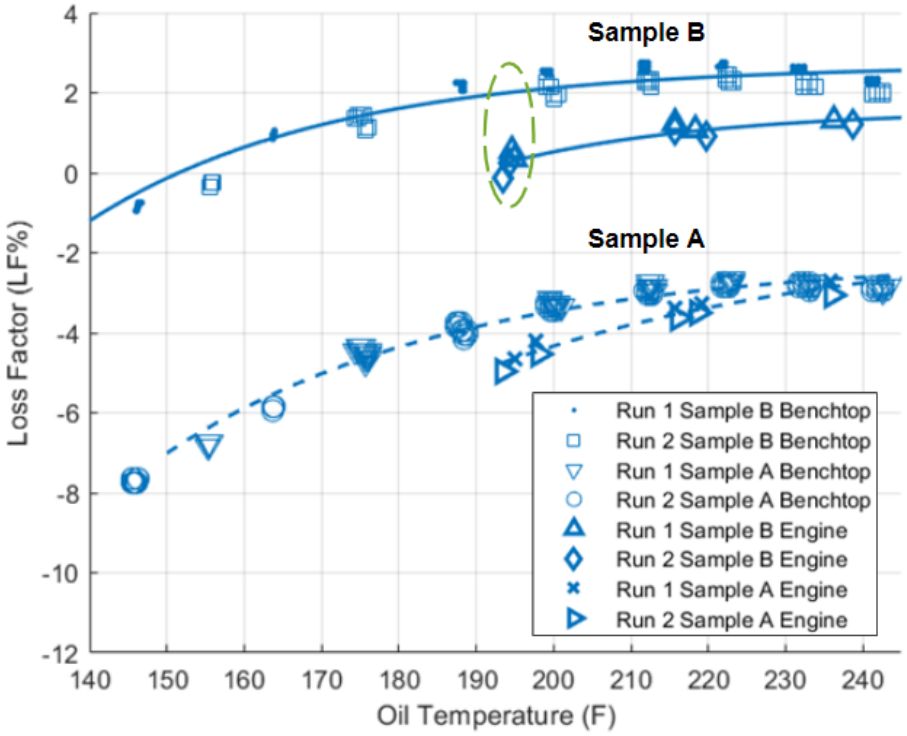

Figure 4.6: Exponential fits for single sensor data from engine and benchtop experiments for both the clean and used oil samples (samples A and B).

4.4 Investigating Aeration as the Root Cause for Measurement Discrepancy

In the flow visualization study, a constant presence of bubbles was observed, with volumetric aeration percentages reaching $\sim$0.1%. The prominent bubble sizes were around 60 µm, which is much smaller than the sampling width of the sensor (Figure 4.7), hinting at the possibility that the continuous presence of these bubbles may influence permittivity-based oil quality sensor assessment. In this context, 0.1% aeration by volume of 60 µm bubbles in a 4L volume of oil amounts to approximately 35 million bubbles.

The presence of air bubbles in the sensor sampling volume could lower loss factor measurements due to the significantly different dielectric properties of oil and air [31] [32]. The flow visualization study also showed that higher viscosity and higher engine speed resulted in higher aeration percentages. The current loss factor measurements corroborate these observations, showing larger differences in loss factor between benchtop and engine measurements at lower temperatures, where the oil viscosity is higher. In the context of used oils, previous studies have shown that the viscosity of lubricating oils increases with use [6] [22] [23]. This increase in viscosity and consequent increase in aeration could potentially result in larger measurement discrepancies as oil deteriorates.

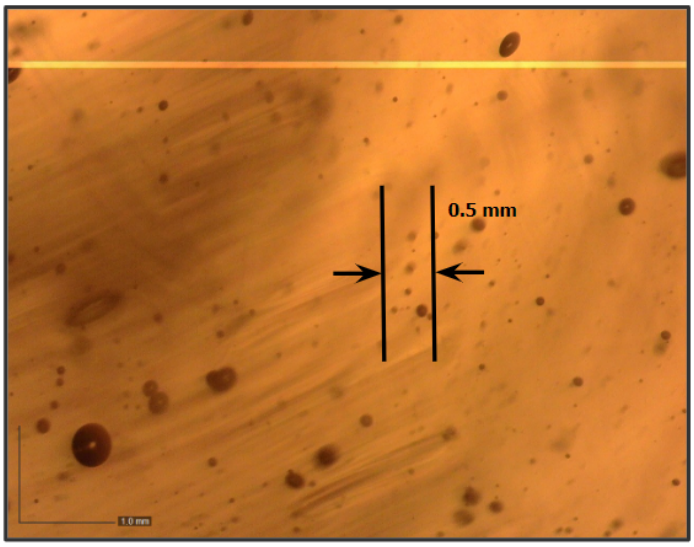

Figure 4.7: Image of aerated oil flow adjacent to the oil filter in the running engine at 220°F, showing prominent bubble sizes compared to the oil quality sensor's capacitor gap size.

The flow visualization studies (Chapter 2) were conducted at a location in the engine prior to the oil filter housing, as post-filter oil drains directly into the engine block and cannot be intercepted. To be able to correlate the pre-filter flow visualization data to the post-filter loss factor OQS measurements, the only viable approach is to compare pre-filter and post-filter OQS loss factor data in a single engine run. Figure 4.8 presents pre-filter and post-filter OQS data for an engine run, showing that the bubbles influencing the measurements are not impeded by the presence of the filter. In this study, sample B had been returned to

the engine that had been flushed with clean oil. The inadvertent effect of blending this used oil sample with residual clean oil in the engine resulted in returning a lower baseline loss factor measurement than that shown in Figure 4.3. This clearly points to the importance of testing engine-extracted oil on the benchtop rather than the other way around, as the engine's residual oil can affect the loss factor measurement of a newly introduced oil.

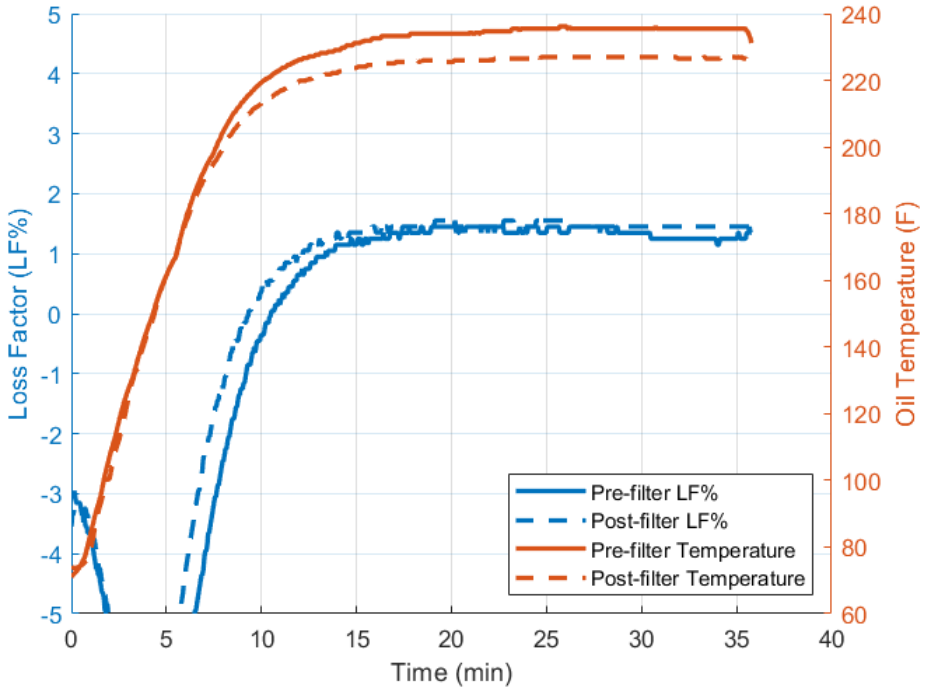

Figure 4.8: Comparison between pre-filter and post-filter OQS loss factor measurements in a single engine run.

Using the data from the flow visualization study, which quantified aeration percentages, and the difference in the loss factor measurements between the engine and the benchtop, a simple linear fit shown in Figure 4.9 has been developed. This fit shows that the difference in OQS measurement increases with aeration percentage; however, the exact dependence should be investigated further.

No flow visualization-based aeration data could be collected for used oil samples due to their opacity; however, due to the increase in viscosity as oil degrades, larger discrepancies would be expected between aerated and non-aerated loss factor measurements in degraded oils. Using the measured differences in loss factor between oil samples A and B (Figure 4.6), an attempt has been made to estimate the aeration percentage of sample B using the linear fit shown in Figure 4.9. According to this preliminary approach, the aeration in used oil sample B could be as high as 0.2%.

It is important to note that the engine data in Figure 4.6 was not taken at a constant engine speed, as

the oil temperature in the engine was resultant from manipulating the engine load and throttle to represent typical power-production engine run conditions. This meant that the higher temperature engine data was collected with the engine operating at higher speeds. The data from the earlier flow visualization studies showed that oil aeration is dependent not only on oil temperature, but also on engine speed. Since the goal of this study was to analyze the oil quality sensor's response to typical engine operating conditions, the engine speed changed concurrently as engine load and throttle changed, since this criterion is more representative of typical engine operation than low-load high-rpm or high-load low-rpm engine run conditions. If all data were taken at the same engine speed (e.g. 2800 rpm) and identical temperatures to those seen in the previous engine data (Figure 4.6), the results would follow a curve similar to the dashed line shown in Figure 4.10. The variation between engine and benchtop measurements would be even larger at lower temperatures, as a higher engine speed at those temperatures would result in larger aeration percentages and therefore a larger sensor bias.

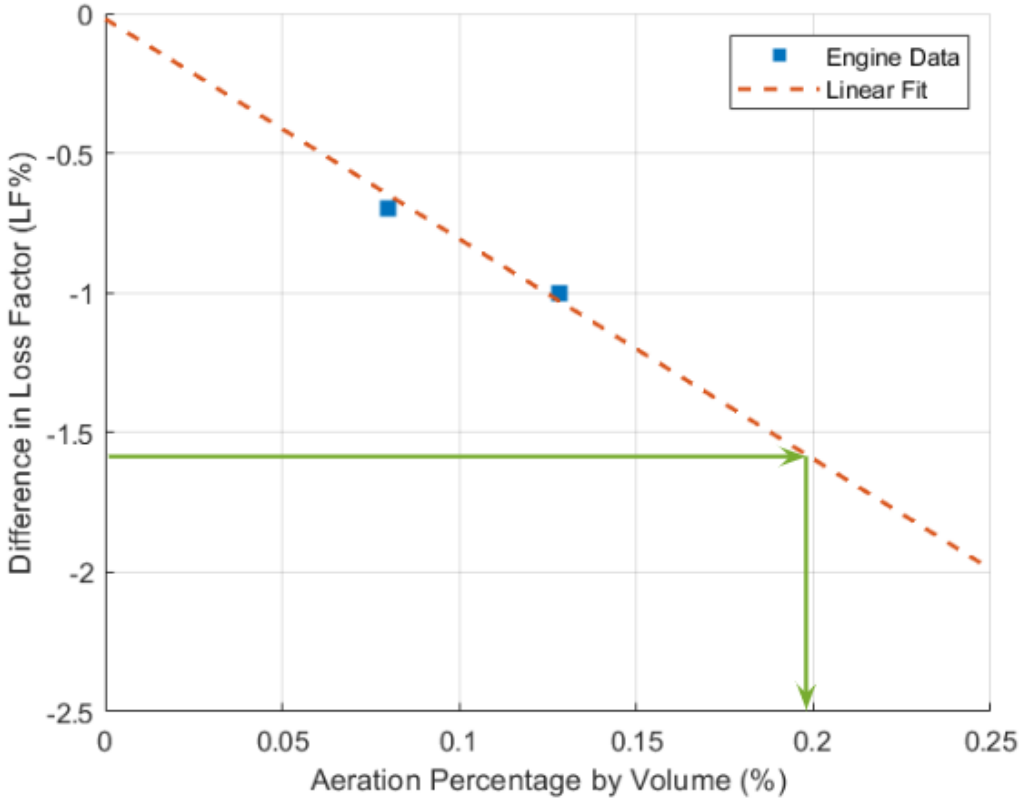

Figure 4.9: Projection for the volumetric aeration percentage from difference in loss factor measurement.

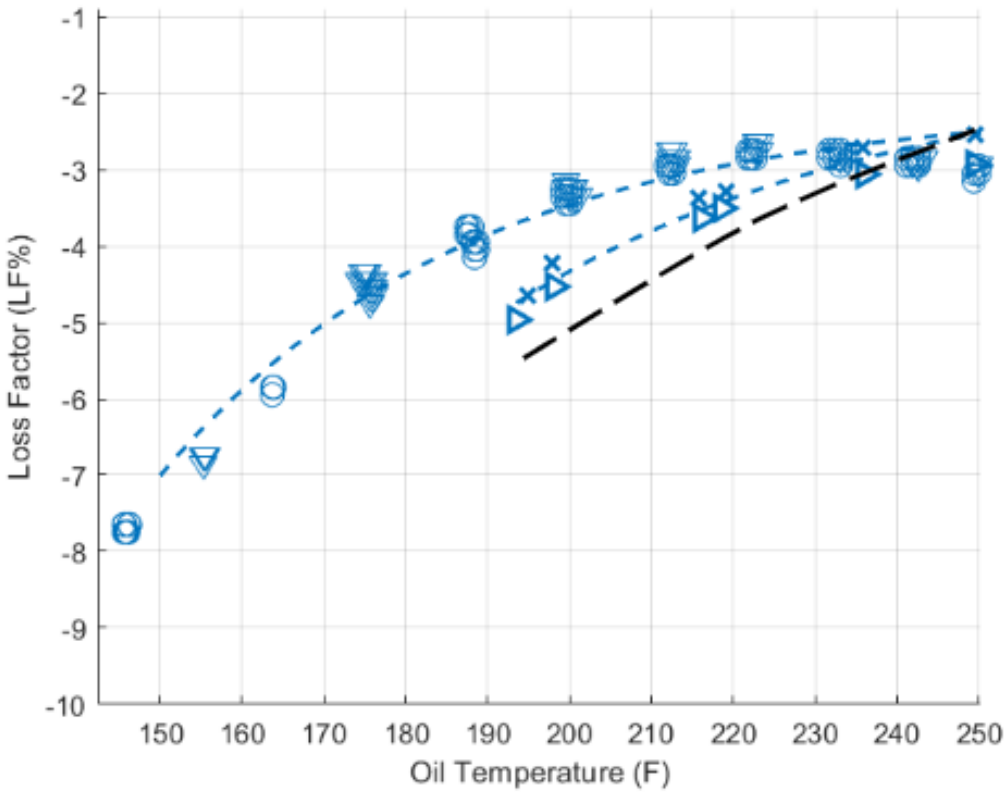

Figure 4.10: Oil sample A (clean oil) benchtop data vs. engine data, with the dashed line qualitatively depicting the results of a study with a constant engine speed of 2800 rpm rather than varying engine speed.

CHAPTER 5

Conclusion

A novel, external flow visualization facility has been developed to optically examine the oil flow characteristics in a running engine at a location prior to the filter. At engine operating conditions ($\sim$220°F), aeration percentages in clean oil flow were found to be in the regime of 0.04% to 0.10%. The most prevalent bubble size was $\sim$60 μm, which is small enough to interfere with the measurements of permittivity-based oil quality sensors. As a working oil ages, surface tension modifiers are depleted and its viscosity increases; both effects can result in increased volumetric aeration. Understanding the aeration characteristics of engine oil flow at a chosen oil quality sensor location will enable proper interpretation of sensor data.

A permittivity-based oil quality sensor was then implemented *in situ* on the diesel engine following its evaluation in a benchtop facility designed to emulate engine operating conditions. In controlled benchtop testing, sensors were verified to be precise within $\pm$0.25 loss factor percentage and agnostic to changes between horizontal and vertical orientations. Oil aeration in the engine caused the sensor's loss factor measurements taken during engine testing to be consistently lower than those taken on the benchtop, and this effect was more pronounced in used oil than clean oil.

This result has implications for *in situ* oil quality sensor implementation, as a sensor submerged in an aerated lubricant flow will return measurements indicating the oil is cleaner (less degraded) than it truly is. To reliably implement real-time permittivity-based oil quality sensing, the oil quality measured in engines must be mapped back to that measured in non-aerated flow using correlations established through controlled aeration experiments.

Another factor to note in real-time sensor implementation is the blending of used oil with clean oil. This will lead to a decrease in the loss factor measurement of the used oil, an effect that could potentially occur in engine testing when a working oil level is topped off with clean oil. Operating the engine at oil levels below those recommended could introduce air into the line, also biasing the results. Another aspect that must be addressed when implementing oil quality sensors is the standardization of loss factor reference values. A clean, non-aerated oil should report a baseline measurement of 0 LF% at engine operating temperatures. By this suggestion, sample C used in this study, adjusted to this baseline, would report a loss factor of near 10 LF%, which considering that it is from an automotive engine with 218,000 miles on its odometer and was run for 8300 miles, would represent near end-of-life for the oil.

References

[1] Zhu, Xiaoliang, Chong Zhong, and Jiang Zhe, "Lubricating oil conditioning sensors for online machine health monitoring – a review," *Tribology International* 109 (2017): 473–84, doi: 10.1016/j.triboint.2017.01.015.

[2] Yadav, B.C., Srivastava, Richa, Dwivedi, C.D., and Pramanik, P., "Moisture sensor based on ZnO nanomaterial synthesized through oxalate route," *Sensors and Actuators B* 131 (2008): 216-222, doi: 10.1016/j.snb.2007.11.013.

[3] Balde, Mamadou, Vena, Arnaud, and Sorli, Brice, "Fabrication of porous anodic aluminum oxide layers on paper for humidity sensors," *Sensors and Actuators B* 220 (2015): 829-839, doi: 10.1016/j.snb.2015.05.053.

[4] Ulrich, Christian, Petersson, Henrik, Sundgren, Hans, Björefors, Fredrik, and Krantz-Rülcker, Christina, "Simultaneous estimation of soot and diesel contamination in engine oil using electrochemical impedance spectroscopy," *Sensors and Actuators B* 127 (2007): 613-618, doi: 10.1016/j.snb.2007.05.014.

[5] Markova, L.V., Myshkin, N.K., Kong, H., and Han, H.G., "On-line acoustic viscometry in oil condition monitoring," *Tribology International* 44 (2011): 963-970, doi: 10.1016/j.triboint.2011.03.018.

[6] Jakoby, Bernhard, Scherer, Monika, Buskies, Matthias, and Eisenschmid, Heinz, "An automotive engine oil viscosity sensor," *IEEE Sensors Journal* 3, no. 5 (October 2003): 562-568, doi: 10.1109/JSEN.2003.817164.

[7] Halalay, Ion C., Schneider, Eric W., "In-situ monitoring of engine oils through electrical AC impedance measurements," SAE Technical Paper 2007-01-4092, 2007, doi: 10.4271/2007-01-4092.

[8] Pérez, Angel T. and Hadfield, Mark, "Low-cost oil quality sensor based on changes in complex permittivity," *Sensors* 11 (2011): 10675-10690, doi: 10.3390/s111110675.

[9] Jun, Hong-Bae, Kiritsis, Dimitris, Gambera, Mario, and Xirouchakis, Paul, "Predictive algorithm to determine the suitable time to change automotive engine oil," *Computers & Industrial Engineering* 51 (2006): 671-683, doi: 10.1016/j.cie.2006.06.017.

[10] Zakarian, Jack and Webber, Clive, "Oxidation of axle lubricants – laboratory studies and a model to predict service life," *SAE Int. J. Fuels and Lubricants* 7, no. 3 (2014): 901-910, doi: 10.4271/2014-01-2801.

[11] Boullosa, David, Larrabe, Juan L., Lopez, Alberto, and Gomez, Miguel A., "Monitoring through T2 Hotelling of cylinder lubrication process of marine diesel engine," *Applied Thermal Engineering* 110 (2017): 32-38, doi: 10.1016/j.applthermaleng.2016.08.062.

[12] Ventikos, Nikolaos P., Sotiralis, Panagiotis, and Annetis, Emmanouil, "A combined risk-based and condition monitoring approach: developing a dynamic model for the case of marine engine lubrication," *Transportation Safety and Environment* 4, no. 3 (2022), doi: 10.1093/tse/tdac020.

[13] Kimura, Yusuke, Kato, Naoya, Kataoka, Takahashi, Katsuaki, and Kikuchi, Takashi, "Bubble behavior in engine lubricant," *International Journal of Automotive Engineering* 2 (2011): 149-153, doi: 10.20485/jsaeijae.2.4_149.

[14] Deng, Q., Anilkumar, A.V., and Wang, T.G., "The role of viscosity and surface tension in bubble entrapment during drop impact onto a deep liquid pool," *J. Fluid Mechanics* 578 (2007): 119-138, doi: 10.1017/S0022112007004892.

[15] Fowle, T.I. "Aeration in lubricating oils," *Tribology International* 14, no. 3 (1981): 151–157, doi: 10.1016/0301-679x(81)90062-1.

[16] Manz, D. L., Cowart, J. S., and Cheng, W. K., "High-speed video observation of engine oil aeration," SAE Technical Paper 2004-01-2913, 2004, doi: 10.4271/2004-01-2913.

[17] Nemoto, Shuzo, Kawata, Kunihiko, Kuribayashi, Toshiaki, Akiyama, Kenyu, Kawai, Hiromi, and Murakawa, Hideki, "A study of engine oil aeration", *JSAE Review* 18, no. 3 (July 1997): 271-276, doi: 10.1016/S0389-4304(97)-00008-8.

[18] Baran, Bridget and Cheng, Wai K., "Assessing the windage tray blockage effect on aeration in the oil sump," SAE Technical Paper 2007-01-4109, 2001, doi: 10.4271/2007-01-4109.

[19] Manz, Devon and Cheng, Wai K., "On-line measurements of engine oil aeration by X-ray absorption," *J. Eng. Gas Turbines Power* 129, no. 1 (Jan. 2007): 287-293, doi: 10.1115/1.2360604.

[20] Smith, Adam D. and Anilkumar, Amrutur V., "Friction factor evaluation of replaceable-element and conventional oil filters in a precision benchtop test facility," *SAE Int. J. Fuels and Lubricants* 15(3):2022, doi: 10.4271/04-15-03-0012.

[21] Kerho, Michael F. and Bragg, Michael B., "Neutrally buoyant bubbles used as flow tracers in air," *Experiments in Fluids* 16 (1994): 393-400, doi: 10.1007/BF00202064.

[22] George, Sam, Balla, Santhosh, Gautam, Vishaal, and Gautam, Mridul, "Effect of diesel soot on lubricant oil viscosity," *Tribology International* 40, no. 5 (2007): 809-818, doi: 10.1016/j.triboint.2006.08.002.

[23] Agoston, A., Ötsch, C., and Jakoby, B., "Viscosity sensors for engine oil condition monitoring – Application and interpretation of results," *Sensors and Actuators A* 121 (2005): 327-332, doi: 10.1016/j.sna.2005.02.024.

[24] Agoston, A., Schneidhofer, C., Dörr, N., and Jakoby, B., "A concept of an infrared sensor system for oil condition monitoring," *Elektrotechnik & Informationstechnik* 125 (2008): 71-75, doi: 10.1007/s00502-008-0506-3.

[25] Zhan, Che, Saint-Jalmes, A., Receveur, M., El Bahi, H., Rondelez, F., and Leroy, V., "Detailed characterization of aeration in lubricating oils by an ultrasonic approach," *Tribology International* 175, no. 107782 (2022), doi: 10.1016/j.triboint.2022.107782.

[26] Dervos, Constantine T., Paraskevas, Christos D., Skafidas, Panayotis D., and Vassiliou, Panayota, "A complex permittivity based sensor for the electrical characterization of high-voltage transformer oils" *Sensors* 5, no. 4 (2005): 302-316, doi: 10.3390/s5040302.

[27] Botterill, Sam and Greenwood, Chris, "Real time oil condition monitoring, practical examples of trend analysis & failure prevention," Paper presented at 17th Australian Aerospace Congress, Melbourne, Australia, 26-28 February, 2017.

[28] Basu, Amiyo, Berndorfer, Axel, Buelna, Carlos, Campbell, James et al., "'Smart sensing' of oil degradation and oil level measurements in gasoline engines," SAE Technical Paper 2000-01-1366, 2000, doi:10.4271/2000-01-1366.

[29] Clark, Ryan J. and Fajardo, Claudia M., "Assessment of the properties of internal combustion engine lubricants using an onboard sensor," *Tribology Transactions* 55, no. 4 (2012): 458-465, doi: 10.1080/10402004.2012.670892.

[30] Byington, Carl, Argenna, Garrett, Mackos, Nicholos, Ruestow, Andrew, and Schmitigal, Joel, "Development and testing of an online oil condition monitor for diesel driven army ground vehicles," SAE Technical Paper 2012-01-1348, 2012, doi:10.4271/2012-01-1348.

[31] Corach, J., P.A. Sorichetti, and S.D. Romano. "Electrical properties of vegetable oils between 20 Hz and 2 Mhz." *International Journal of Hydrogen Energy* 39, no. 16 (2014): 8754–8758, doi: 10.1016/j.ijhydene.2013.12.036.

[32] Carey, A. A. “Dielectric constant and oil analysis.” *Machinery Lubrication*, June 27, 2019, url: https://www.machinerylubrication.com/Read/226/dielectric-constant-oil-analysis.

[33] Looyenga, H., “Dielectric constants of heterogeneous mixtures,” *Physica* 31, no. 3 (1965): 401-406, doi: 10.1016/0031-8914(65)90045-5.

[34] Wrasse, Aluisio do, Vendruscolo, Tiago P., Santos, Eduardo N.d., Pipa et. al., “Capacitive multielectrode direct-imaging sensor for the visualization of two-phase flows.” *IEEE Sensors Journal* 17, no. 24 (2017): 8047–8058, doi: 10.1109/jsen.2017.2724063.

[35] Smith, Adam D., “Design of a benchtop facility for parametric evaluation of engine oil quality,” Master of Science Thesis, Vanderbilt University, 2021.